

UNCLASSIFIED

AD NUMBER

AD895214

LIMITATION CHANGES

TO:

Approved for public release; distribution is unlimited.

FROM:

Distribution: Further dissemination only as directed by Naval Ordnance Lab., White Oak, MD, 04 JAN 1951, or higher DoD authority.

AUTHORITY

Naval Ordnance Lab ltr, 26 Aug 1974

THIS PAGE IS UNCLASSIFIED

NAVORD REPORT

31839
AUG 1 1965
JUN 8 1966
FEB 24 1966

NOL HYPERBALLISTICS TUNNEL NO. 4 RESULTS I: - AIR LIQUEFACTION

LIBRARY OF CONGRESS
REFERENCE DEPARTMENT
TECHNICAL INFORMATION DIVISION
FORMERLY
NAVY RESEARCH SECTION

4 January 1951

JUL 17 1962

PLEASE RETURN THIS COPY TO:

ARMED SERVICES TECHNICAL INFORMATION AGENCY
DOCUMENT SERVICE CENTER
Knott Building, Dayton 2, Ohio

Because of our limited supply you are requested to return
this copy as soon as it has served your purposes so that
it may be made available to others for reference use.
Your cooperation will be appreciated.



U. S. NAVAL ORDNANCE LABORATORY
WHITE OAK, MARYLAND

AEDC TECHNICAL LIBRARY



5 0720 00045 3730

CATALOGED BY ASTIA
98387
ATI NO. 98387
AS

Aeroballistic Research Report 19

NOL HYPERBALLISTICS TUNNEL NO. 4 RESULTS I: AIR LIQUEFACTION

Prepared by:

P. Wegener

E. Stollenwerk

S. Reed

G. Lundquist

ABSTRACT: Since the presence of condensed air in a hypersonic wind tunnel can make the operation of the tunnel difficult, and since liquefaction can occur when the temperature and pressure in the test section are below the condensation values, an investigation was carried out on the liquefaction of air in a hypersonic wind tunnel. The tunnel used was built to operate at Mach numbers up to 11. The liquefaction was investigated under conditions in which the temperature and pressure of the supply air could be varied. It was found that air, unlike water vapor, does not supersaturate and heating of the supply air is required for satisfactory operation of a hypersonic wind tunnel. Experimental measurements show that a portion of the air condenses at or shortly after it reaches the predicted conditions for equilibrium-saturation in the nozzle. Since the presence of liquefaction may affect standard methods of measuring the Mach number of the flow in the tunnel, the response of these standard methods to liquefaction was examined. It was found that pitot-tube determinations of Mach number are relatively insensitive to air liquefaction whereas determinations using static pressures and shock-wave angles that are produced by slender bodies vary with the amount of air condensation. By maintaining a high temperature in the supply air the various standard methods for measuring the Mach number were found to give consistent Mach number data. The minimum temperature required to achieve this consistency appeared to be smaller than the value calculated on the assumption that a disturbing amount of condensation appears when the condition for equilibrium saturation is reached.

The absence of air supersaturation is explained on the assumption that large numbers of condensation nuclei of beyond critical size are available because of the condensation of a small amount of CO_2 and water vapor present in the tunnel air. In the analysis it is assumed that after the air reaches the condition of equilibrium-condensation a saturated isentropic expansion takes place. It was possible to estimate the fraction of air which condenses under the operating conditions of the tunnel.

U. S. NAVAL ORDNANCE LABORATORY
WHITE OAK, MARYLAND

An explanation is also advanced using the same assumption and analysis to explain why the pitot tube pressures are not very sensitive to air condensation. The theoretical analysis shows that some of the dimensionless flow parameters deviate markedly from the value expected without liquefaction, while others are nearly the same regardless of liquefaction.

Flows with preheated air in the NOL 12 x 12 cm Hyperballistics Tunnel No. 4 which are sufficiently free of liquefaction to carry out model testing were obtained with Mach numbers as high as 8.25. The unique features of wind-tunnel design and instrumentation which contributed to this accomplishment are also contained in this report.


NAVORD Report 1742

4 January 1951

This is the first NAVORD report on an investigation carried out in the new Hyperballistics Wind Tunnel No. 4 located at the U. S. Naval Ordnance Laboratory, White Oak, Maryland. This wind tunnel was sponsored by the Bureau of Ordnance and was put into operation in May 1950. The major portion of this report is on air liquefaction. The particular task reported here was recommended by the NOL Advisory Aeroballistics Panel under Aeroballistic Research Request No. 95, and was carried out under NOL task number NOL-4-Re9a-108-1-51. The work is being continued.

The authors wish to thank Mr. H. Staab who participated in the design, instrumentation, and operation of the tunnel. Miss D. Ericson assisted in taking and evaluating the data. Many discussions with co-workers in this field during the last years were stimulating and assisted this project greatly. In particular, the exchange of results and ideas with the group at Princeton University under Professor L. Lees and that at CIT under Dr. H. Nagamatsu is gratefully acknowledged.

W. G. SCHINDLER
Rear Admiral, USN
Commander


R. J. SEEGER, Chief
Aeroballistic Research Department
By direction

CONTENTS

	Page
I. Introduction	1
II. Operation at High Mach Numbers	1
III. General Discussion of the Air Liquefaction Problem	3
IV. Air Liquefaction Results	6
V. Proposed Interpretation of the Condensation Process	9
VI. List of References	14

APPENDIX

I. Thermodynamic Analysis of Condensation Process	16
II. Design and Operation of NOL 12 x 12 cm Hyperballistics Tunnel No. 4	21
III. Instrumentation	24

NOL HYPERBALLISTICS TUNNEL NO. 4 RESULTS I: AIR LIQUEFACTION

I. INTRODUCTION

1. One phase of this Laboratory's hypervelocity research program is its hyperballistic tunnel research. Here the term hyperballistic refers loosely to flow phenomena in the range of Mach numbers above five. The present phase of the program may be divided into two steps, namely,

a. the investigation of techniques for obtaining uniform flow at high Mach numbers in wind tunnels, and

b. the carrying out of a research program in aeroballistics at high Mach numbers.

2. This report is an account of the results obtained in step (a) with special reference to the problem of air liquefaction.

3. The present tunnel was put into operation in May 1950. Some of the mechanical difficulties encountered in the development of the tunnel, especially those arising from the high supply temperatures and pressures, are also discussed in this report.

4. Details of a thermodynamic analysis, certain technical aspects of the tunnel and the instrumentation can be found in the appendices.

II. OPERATION AT HIGH MACH NUMBERS

5. The operation of the tunnel can be followed by referring to Figures 1, 2, and 3. In order to obtain hypersonic flow, large over-all pressure ratios are necessary. In the present tunnel a pressure ratio of 50,000 is available. Because of this, diffuser efficiency is not important and is not discussed in this report.

6. The "wedge nozzle" shown in Fig. 3 was designed to permit a quick change of Mach number over a wide range by means of changes in the area-ratio as described in Appendix II. This arrangement was considered indispensable for an investigation which had to do primarily with physical phenomena occurring in the flow under a wide variety of flow conditions rather than with aerodynamic testing at a fixed Mach number.

7. The following observations indicate that the flow in a slender wedge nozzle (50 cm length and 12 cm final width) can be treated as one dimensional:

a. A value of Mach number obtained from area-ratio data using one-dimensional theory was compared with the value obtained by applying the method of characteristics and found to be compatible. This is clear from values for the centerline of the nozzle shown in Fig. 4. The two sets of Mach number data are nearly equal.

b. Applying the method of characteristics to the flow in the nozzle also shows that the change in Mach number, from wall-to-wall at the nozzle exit, is of the same order as the accuracy of experimental Mach number determination from, say, measurement of static pressures.

c. The last fact is borne out by the ratio of pitot pressure p'_o to supply pressure p_o ; i.e., p'_o/p_o , as measured across the nozzle exit with 3 pitot tubes, spaced 3 cm from each other; the ratio is nearly constant, as is evident from Fig. 5. The nozzle was set for the area-ratio corresponding to a Mach number of 7.6, $p_o = 7$ atm and $T_o =$ room temperature. The thickness of the boundary layer for this situation is about 1.5 cm.

8. The wide variety of supply conditions used in the investigation gives rise to an equally wide variety of boundary layer thicknesses. Simple fitting of the nozzle blocks permits boundary layer corrections.

9. For model testing, the wedge nozzle has the disadvantage that it does not yield uniform flow in the test section. However, for short models, of about 5 cm length, the Mach number variation near the nozzle end is small enough to permit survey work.

10. A small change in the cross-sectional area at the throat has a considerable effect on Mach number at the nozzle exit. Two causes of throat changes were examined and the following observations made:

a. When the supply pressure was varied over the range from 1 to 8 atm, Mach number determined at the nozzle end did not vary significantly. This means that spreading of the nozzle walls at the throat due to air pressure in this range is negligible.

b. At high supply temperature, the nozzle surface at the throat is heated, and the cross-sectional area is reduced. The magnitude of this effect depended on the duration of the test, on the throat area, and on the manner of heating the supply air (e.g., preheating through tunnel or by-pass). The throat opening was measured by means of feeler gages, before and after each test.

11. As a consequence of heating, the temperature of the surfaces of the nozzle and the wall increased in the course of a run. Even for $T_o = 150^\circ\text{C}$ temperatures measured on the outside of the tunnel did not stabilize fully during 2 hours of continuous operation. (It is noteworthy that no window breakage occurred even during long runs at high supply temperature.

This may be due, in part, to poor heat transfer at the low test-section densities.)

12. The limited size of the test-section and the difficulties of instrumentation both give rise to a practical upper limit of Mach number at about $M = 11$. (The separation of throat walls is then only 0.2 mm.) The shock waves from slender test bodies are hardly visible in the schlieren pictures at $p_0 = 8$ atm. The photographs shown in this report are of poor quality, partly because the glass for the windows was selected to withstand heating and did not have good optical properties. Besides, with the heating there is considerable convection of air outside the test section, which obscures details.

13. At the same $M = 11$ setting, pitot pressures were measured on the nozzle centerline at the exit. The Mach number determined in the conventional manner from the ratio of pitot pressure to supply pressure was 10.4. Schlieren pictures of a 40° and 80° cone-cylinder and a 40° wedge are shown for this condition on Fig. 6.

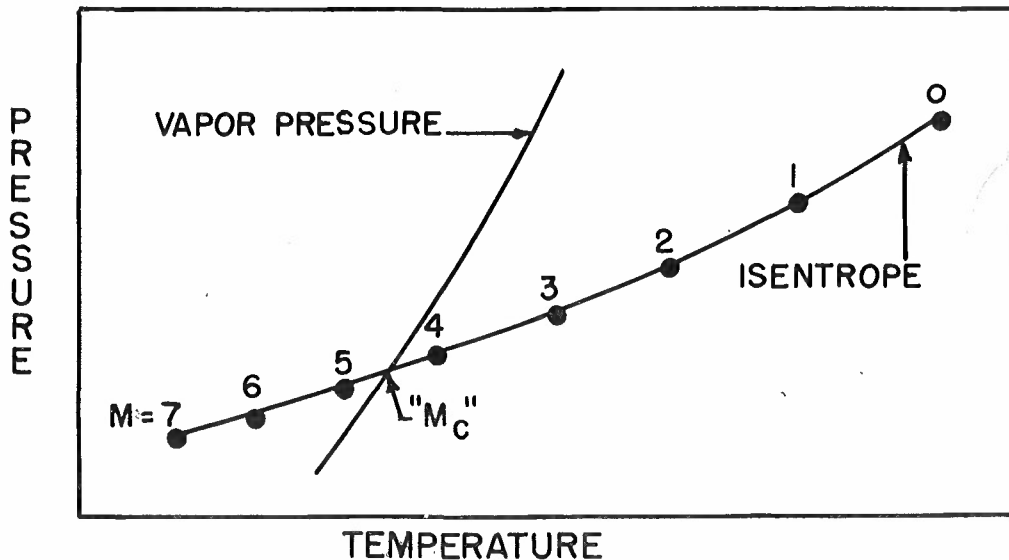
14. A plot of Reynolds number per unit length, computed in the ordinary way for the range of conditions of the tests reported here, is given in Fig. 7. To obtain data from Fig. 7 for $p_0 > 1$ atm, multiply (Re/cm) for a given M and T_0 by p_0 in atm.

15. The air provided for the tunnel is believed to be reasonably free of dust. A high-pressure filter is used to remove oil droplets. A high-pressure jet blowing on cheesecloth leaves no deposit which can be detected with a microscope. No oil condensate can be observed on a stainless steel mirror surface which has been exposed to this jet. The air is dried to a dew point less than $-50^\circ F$ (at 1 atm pressure), which indicates that there is less than 0.04 g H_2O per gram of air. No attempt was made to remove CO_2 from the air.

III. GENERAL DISCUSSION OF THE AIR LIQUEFACTION PROBLEM

16. If the expansion of air in the wind tunnel is an isentropic expansion of a perfect gas, pressure and temperature will decrease, as depicted by the curve designated as "isentropes" in Sketch 1. Supply conditions, corresponding to the point O, are held fixed. A scale of Mach numbers, obtained from perfect gas isentropes tables, e.g. reference (a), is marked off on this curve. The vapor-pressure curve for air, extrapolated from experimental data (reference b) will intersect the expansion isentropes at some point, which can be identified by the corresponding Mach number M_c . This value identifies a Mach number above which the danger of air liquefaction begins. Hence M_c is called the "Mach number of equilibrium condensation" (reference c).

Sketch 1: Pressure-Temperature Diagram



17. If the supply conditions at the point 0 are atmospheric pressure and 15°C, the value of M_c is 4.8.

18. From the trend of the two curves in Sketch 1, it appears that M_c can be increased by decreasing p_0 and/or increasing T_0 . Estimates of values of M_c , as functions of p_0 and T_0 , based on the same assumptions used in Sketch 1, were made in reference (c) and are given in Fig. 8.

19. It is undesirable to decrease the supply pressure since high supply pressures are necessary in order to:

- a. obtain acceptable test-section pressures and model forces,
- b. maintain sufficiently large density in the test section so that slip flow effects do not occur, and
- c. maintain a density large enough to permit the use of optical methods.

20. Increasing T_0 is feasible within limits set by practical difficulties. For example, to operate at $M_c = 10$ with $p_0 = 100$ atm, requires that T_0 be about 1000°K. Serious technical problems must be overcome to heat air to these high temperatures and high pressures.

21. Hence, interest has turned to an investigation of flow phenomena that takes place when supply temperatures are not high enough and the criterion M_c is not realized.

22. There was some expectation that the air would supersaturate in the wind tunnel expansion. This seemed to be verified by results of tests performed with a small wind tunnel at Princeton University (reference d). Moreover, the experience with water-vapor expansions pointed to this conclusion.

23. It was well known that water-vapor, expanding as steam in turbine nozzles, or expanding together with air in supersonic wind tunnels, followed a "dry isentrope" well beyond saturation, and then condensed suddenly, giving rise to a so-called "condensation" shock (references c, e, f, and g). In tests performed at NOL with a 2.5 x 2.5 cm wind tunnel, for example, water vapor was found to undergo a "dry" isentropic expansion 80 to 100 degrees beyond its saturation point, (reference h).

24. Equally well known was the fact that water vapor supersaturates when expanded quickly in cloud chambers. Some recent results of Cwilong (reference i) are of particular interest in this respect. He found that if moist air, from which foreign nuclei were removed by filtering, was expanded "rapidly" in a cloud chamber to a temperature below 150°K, condensation could not be observed. Head (reference g) found the same phenomenon in a supersonic wind tunnel.

25. Two of the authors, however, using a sensitive electronic method for detecting the light scattered from droplets, found that moist air which was expanded "very quickly" in a shock tube definitely contains droplets.

26. A successful account of the occurrence and strength of water-vapor condensation shocks in nozzle flow was given by Oswatitsch (reference j) using the theory of Becker, Doering and Volmer (reference k) which assumes the condensation process to be not affected by foreign nuclei. Calculations for air condensation, made on the same basis as those of Oswatitsch, predicted a considerable supersaturation in the wind tunnel expansion.

27. These expectations of air supersaturation were not observed in the tests described in this report. Rather, our results agree with those found at the NACA, Langley, with the 10" hypersonic tunnel by C. H. McLellan, reference (1), which indicate that air liquefaction effects do occur very near the saturation-point. At low supply temperatures, our results agree also with those found with the 5" CIT hypersonic tunnel by Nagamatsu and his group (reference m).

28. An explanation of this absence of supersaturation is that large numbers of foreign nuclei beyond the "critical size" are present. In fact simple calculations, given below, show that the condensation, in the early stages of expansion, of a small fraction of the CO₂ and/or of the rest of the water vapor present in the air in the wind tunnel would supply a sufficient quantity of such nuclei.

29. On the assumption that the condensation takes place reversibly beginning at the saturation point of air, thermodynamic theory was applied to the expansion process, and an estimate was made of the fraction of the air that is condensed.

IV. AIR LIQUEFACTION RESULTS

30. The data on air liquefaction effects are presented in Figs. 9 to 27 inclusive. The Mach number evaluations shown in these figures are conventional, i.e., values of M are computed by using experimental data together with isentropic flow tables.

A. Pressure Measurements

31. Static pressure measurements made along the nozzle wall for three different nozzle settings are given in Figs. 9, 10, and 11. Two types of static pressure data were obtained for each nozzle setting; namely, with supply temperature T_0 of the order of room temperature (called a "cold run") represented by open circles in the figures, and with T_0 at least equal to T_{0c} , that supply temperature for M_c equals the Mach number of the nozzle setting. This "hot run" is represented by solid circles on the figures. The static pressures for potential flow in the nozzle are shown as dotted curves. The discrepancy between the "hot" static pressure and that of the potential flow may be attributed to the boundary layer.

32. Figure 10 shows static pressure data obtained on two "cold" runs and one "hot" run. For one of the cold runs (triangles), the supply density was equal to that of the "hot" run. For the other, p_0 was equal to that of the "hot" run. The agreement between those two "cold" runs shows that Reynolds number effects are secondary in this range.

33. During the course of a run the nozzle throat becomes gradually heated causing it to close. Therefore, Fig. 11 exhibits two limiting potential-flow curves, corresponding to a "cold" throat ($M = 7.6$), and the "hot" throat measured at the end of the run ($M = 7.9$). In this case the measurements were made point-by-point beginning with the nozzle exit and proceeding towards the throat. Considerably smaller changes took place in the potential-flow curves for Figs. 9 and 10, where only the "cold" throat potential flow is shown. Figure 11 shows in addition Mach numbers evaluated from pitot pressure measurements on the centerline (crosses) for a "cold" run. M agrees here with that from "hot" static pressure measurements.

34. Figure 12 shows the pitot pressure p_0' measured at the center of the nozzle exit plane as function of the supply temperature T_0 . Evidently p_0' is rather insensitive to changes in T_0 throughout the T_0 -range where liquefaction effects may be expected. The dotted curve marked "potential

flow" was obtained from nozzle throat measurements before and after the run by arbitrarily assuming a linear rate of decrease in throat cross-sectional area during the run.

35. Figure 13 shows data on the ratio of static pressure to supply pressure, measured at the nozzle end, as function of supply temperature T_0 , for the $M = 7.6$ setting of the nozzle. Between the lowest and highest values of T_0 the static pressure decreases by a factor 2. These data were taken from 9 different runs. The pressure measurements were made either at the wall or on the centerline, with silicone oil, butyl phthalate or McLeod manometers at increasing or decreasing T_0 . Static pressures measured on the centerline seemed to be slightly higher than wall pressures, but the discrepancy was of the order of the reproducibility.

36. Figure 14 shows pitot and static pressures measured at the nozzle exit, for the $M = 6$ setting. The scale is expanded because the effect of changing T_0 is much smaller.

37. Figures 15 to 20, inclusive, were obtained by a conventional Mach number evaluation using nozzle-exit data. On these figures the value of M_c is given by the dotted curves marked "saturation".

38. For the $M = 7$ setting, data taken under three different supply conditions are presented in Figs. 16, 17, and 18. First the supply pressure was kept constant, and for each fixed value of T_0 two static pressure measurements were taken at an interval of one minute (Fig. 16). Then the Reynolds number, obtained from Fig. 6 was kept constant (Fig. 17). Finally the supply density was held constant (Fig. 18). The results of these tests do not differ significantly. For this reason the discrepancies in M -evaluations can be attributed to liquefaction effects.

39. All previous nozzle exit data for the $M = 7.6$ setting together with data on cone-pressures, are collected on Fig. 19. Readings were taken on two opposite points of the cone surface. The Mach number was evaluated from the ratio of cone surface pressure to ambient pressure (reference n). That the two readings are different is either due to flow inclination or to a misalignment of the model.

40. Figure 20 shows M as computed from pressure data at the nozzle exit for a $M = 9$ setting. Although $T_{oc} = 430^\circ\text{C}$, approximate agreement between the two M evaluations from static and pitot pressures is reached at 300°C .

41. Table I summarizes the nozzle exit results from the "cold" runs. The disagreement in M grows with the Mach numbers of the nozzle setting. This is to be expected, since the liquefaction effects increase as the nozzle-setting Mach number exceeds M_c , which was roughly 4.6 for all these tests.

TABLE I
Mach Number Determinations

M - From Area Ratio	M = From Pitot pressure (p_o'/p_o)	M = From Static pressure (p/p_o)	M = From Rayleigh Formula (p_o'/p)	p_o (atm)
6.00	5.60	5.53	5.39	3.0
7.00	6.65	6.10	5.07	5.0
7.60	7.10	6.44	5.20	7.1
9.00	8.07	7.12	5.37	7.8

B. Shock Angles on Bodies

42. A desirable direct Mach number evaluation would be obtained by making a "Mach line" visible. It was found, however, that because of the low density in the test section any disturbance which can be "seen" with the schlieren system is "strong", i.e., a shock wave. This leaves us with the indirect method of inferring the Mach number from the shock angle on simple bodies, such as the wedge and the cone. If flow conditions are changed a decrease in shock angle indicates an increase of Mach number. (References n, o.)

43. Figure 21 shows a series of schlieren photographs of a 10 degree wedge taken at the $M = 7$ nozzle setting. The supply density was kept constant to minimize differences in index of refraction for different supply temperatures. Using the (accidental) bubble in the glass window as a reference mark, it can be seen that the shock angle decreases with increasing T_o . The shock angles measured by two independent observers are plotted in Fig. 22. The inequality in shock angle on the two sides of the wedge is again due to either flow inclination or misalignment of the model of the order $1/3$ degree.

44. The shock waves found on a 40 degree cone, 80 degree cone, and a sphere were each photographed at three different supply temperatures at the $M = 7.6$ setting and are shown in Figures 23, 24, and 25. The shock angle evaluation by different observers, is shown for cones in Figure 26. The shock angle on the 40 degree cone decreases with increasing T_o . The data from the 80 degree cone are inconclusive, as also were all cases of "strong" or nearly normal shocks such as those produced on a sphere. In fact, examination does not reveal any observable change in the shock wave pattern around the sphere due to elimination of liquefaction.

45. From these photographs it appears that

(1) shock wave angles on slender bodies for a given nozzle setting decrease as T_o is increased, and

(2) the shock wave configurations on blunter bodies are insensitive to liquefaction. (Compare references p and g.)

C. Light Scattering

46. The method of detecting small particles in flows by light scattering (reference r) was first used by Stodola (reference t) with steam many years ago.

47. Figure 27 shows photographs obtained in our tunnel of a narrow beam of light traversing the test section. The reflections from the two windows appear as bright spots. Scattered light can be seen at low values of T_0 ; no signal is visible in the case of "no blow" or at high supply temperatures. The strength of the scattered signal is also dependent upon the intensity of the collimated light beam and the exposure time of the photograph. The relative photographic density of the scattered light is shown in Fig. 27. The densitometer reading merges with the background signal for supply temperatures of about 75°C . If the light beam is moved into the boundary layer during a "cold" run, the scattering disappears. From this it may be concluded that dust, if present, does not cause the scattering. Since large amounts of H_2O and CO_2 droplets or crystals are present in the test section and since these H_2O and CO_2 droplets or crystals are also reduced in number by heating, such light scattering experiments are not regarded as conclusive evidence of air liquefaction and were not pursued further.

48. One effect which might influence the accuracy of the data presented in this report deserves mention. An investigation of cross sections of the flow by using a pitot rake showed, that at comparatively supply densities these profiles possessed irregularities tentatively identified as a flow separation. Figure 28 gives two such profiles obtained with different supply densities, one with and one without separation. Measurements at right angles to the first-mentioned survey gives evidence that this effect is essentially two-dimensional.

49. It could be shown, however, that separation occurs with or without liquefaction and is a function of supply density only, disappearing above about $p_0/p_{\text{atm}} = 4$. The same type of pitot profile with separation was observed in the CIT hypersonic tunnel by Nagamatsu with liquefaction at low supply density.

V. PROPOSED INTERPRETATION OF THE CONDENSATION PROCESS

50. It will first be shown that the heat-release due to condensation of the rest-amount of water vapor and the CO_2 present in the wind tunnel supply air, does not have any measurable effect on the flow. To do this we assume a nozzle setting for $M = 7$, and $p_0 = 7.1 \text{ atm}$ and $T_0 = 16^\circ\text{C}$. The point in the nozzle at which the water vapor will condense can be adequately predicted from references (g) and (h). The "strength" of the

resulting condensation shock, p_2/p_1 , can be computed from the diabatic flow theory, e.g., reference (s). The results of this estimate are shown in Table II assuming a supercooling of 80°C , and a complete condensation of all H_2O or CO_2 . A condensation mechanism similar to that for water vapor was assumed for the carbon dioxide. For dew points of -50°F and below, as used in these tests, the pressure discontinuity due to condensation of H_2O and CO_2 is negligible.

TABLE II
Water Vapor Condensation Shock Strength

Dew point of supply air at 1 atm in $^\circ\text{F}$	Mixing ratio of supply air g H_2O /kg air:	Position of Condensation shock in cm from throat	Pressure ratio across condensation shock
20 (H_2O)	2.14	0.15	1.0930
-20 (H_2O)	.262	0.30	1.0073
-60 (H_2O)	.0214	0.60	1.00125
CO_2	.456	13.50	1.00217

51. A brief examination of the experimental data of expansions with air liquefaction (Figs. 9, 10, and 11) shows that the condensation of air must occur by a process different from that observed for water vapor. Check measurements of static pressure at about 1 cm intervals on the tunnel wall for the 50 cm long nozzle do not reveal strong discontinuities or "air condensation shocks" within the measuring accuracy of about 1 to 3 percent. This difference from the water vapor or steam case can be explained tentatively by simple kinetic considerations. The condensed amount of H_2O and CO_2 present in the nozzle furnishes a large quantity of droplets or crystals which in turn can serve as nuclei for air liquefaction since they are available some distance ahead of the saturation point of air in the nozzle. (Compare location of air saturation in Figs. 9 to 11 with Table II.) Figure 29 provides a rough estimate of the number of such nuclei present per cc at the point of air saturation as a function of droplet radius. This estimate is inaccurate to the extent it assumes that all water vapor is condensed in spherical droplets of equal size. The number of CO_2 droplets is about equal to that of water vapor at the -20° dew-point.

52. Although the exact number of H_2O and CO_2 droplets available at the saturation point of air cannot be estimated without more extensive calculations, it must be "very high". Figure 29 also gives the stable "air droplet" radius as a function of saturation ratio computed from Thomson's formula (e.g., reference g). Although this calculation does not apply for droplet radii smaller than about 10^{-7}cm (reference d), it is adequate for the larger radii. It can be seen that seemingly "small" water vapor or carbon dioxide droplets are beyond this critical "stable" size and

so may promote air liquefaction at or very shortly after the saturation point shown in Figs. 9, 10, and 11. The assumption that a sufficient number of such nuclei is present to permit nearly equilibrium condensation is a basis for simple thermodynamic theory to be used in explaining the observations. A further consequence of this assumption is that there will be considerable practical difficulty in lowering the number of water drop-let nuclei appreciably, because any further air drying on a large scale is extremely difficult. Even complete removal of CO_2 would do little better than cut the total number of nuclei in half. Shock tube experiments presently under way at NOL (reference t) and cloud chamber experiments by Lees' group at Princeton University may shed more light on this question.

53. The experimental data suggest an analysis in which it is supposed that all processes, exclusive of shocks, are reversible. (Reference f.)

54. For background we describe qualitatively an isentropic expansion of a single-component substance which ends in the coexistence region of two phases, vapor and liquid.

55. Figure 30 shows a schematic pressure-volume (specific) diagram of two expansions: one, ODE, proceeding as a perfect gas isentrope from the tunnel supply conditions at O to the "dew point" line CC', thence as the isentropic expansion of a saturated vapor and its coexistent condensed phase to the end point E. The other, ODE', follows the perfect gas isentrope to the end point E'. The points along DE' do not correspond to equilibrium states; those along DE do. The mass fraction condensed, g , at the point J along ODE is given by the ratio of lengths JB'/BB' along the isotherm BB'. As long as the expansion begins at larger (specific) volumes than the critical, and proceeds at least similarly to ODE, g will increase gradually, attaining small values, and will never reach unity.

56. The "dew point" D must be located by means of extrapolated experimental data, and the subsequent mixed-phase expansion DE can be followed with an accuracy which depends on the accuracy of such data.

57. The pressure and temperature along the adiabatic DE must continually decrease, because the adiabatic must always be steeper than the isotherm BB'.

58. As T_0 is raised, the point O, Fig. 30, moves to the right carrying the gas isentrope ODE' with it, and the point D moves to the right also, falling on the relatively flat part of the gas isentrope. Since DE lies between CC' and the gas isentrope, DE', one sees that the expansion along DE will not deviate much from DE' when D falls near the end of the expansion. If the expansions in our nozzle are drawn to scale in a pressure-volume diagram such as Fig. 30, the lines CC', DE and DE' are nearly horizontal, near the end of the expansions. For the starting temperature T_{0c} at which E, E' and D coincide, and for starting temperatures $> T_{0c}$,

no condensation is expected to occur in the expansion. The speed of sound,

$$a = \sqrt{(dp/d\rho)_s}$$

for the saturated expansions can be computed by taking slopes along ODE. (Assignment of a as the speed of sound in the coexistence region involves physical assumptions which are not discussed here.) Figure 31 shows a as a function of volume, and also the quantity $\sqrt{dp/d\rho}$ evaluated from the slope of the curve ODE'. Figure 30 shows that DE' and DE are both nearly horizontal for large values of volume. Their respective slopes, curves DE' and DE in Fig. 31 can eventually intersect as shown. If Mach number M is computed using this speed of sound according to the definition $M = v/a$, where v is the average flow speed, a sharp rise in M may be expected at and after the dew point, D , because a drops sharply and v changes slowly. If one uses pressure values along DE together with tables (reference a), fictitious Mach numbers are obtained which will undergo only a gradual increase at and after D . Due to the sharp drop in a , $M = v/a$ will exceed that obtained from these tables, near the dew point.

59. These remarks apply strictly to the expansion of pure substances, such as N_2 or O_2 . Qualitative use of them can be made for air although air is a multicomponent mixture having a state which depends on its composition as well as its pressure and volume. The vapor pressure and composition of air at the low temperatures and pressures are not known precisely and extrapolation of available data (reference b) is common practice. The precise position of the line CC' is not known, and the expansion DE cannot be followed accurately. A determination of T_{oc} , which depends on knowledge of the position of D and of E and E' in the $p-v$ diagram, is therefore subject to these inaccuracies. In our analysis we assumed air is a fictitious single-component substance having the extrapolated vapor pressures.

60. The experimental behavior of the static pressure, after reaching the dew point, as exhibited for example in Fig. 11, is similar to ODE in Fig. 30, except that the discontinuous jump in slope appearing at D in Fig. 30 is a continuous transition in Fig. 11. (Details of the procedure used in analyzing the data are given in Appendix I.)

61. In the experiments, there were two extremes of supply temperature (see Figs. 9, 10, and 11).

62. To all expansions the equations of continuity and momentum could be applied. From order of magnitude considerations it follows that the ratio of (mass-average) flow speed v to the speed of sound under supply conditions a_0 , i.e., v/a_0 , will be equal to within a few percent for both hot and cold expansions. This implies, according to our assumptions that the ratio h/h_0 of (average) enthalpy of the system, h , to the enthalpy under supply conditions, h_0 , is almost equal for "hot" and "cold" expansions. Also implied is that ρ/ρ_0 , the ratio of density of supply density for

the "hot" and "cold" expansions, are inversely proportional to their respective effective areas.

63. The mass fraction condensed, g , was computed, with results shown in Fig. 33. A graph of pressure versus density was then plotted from which sound speed,

$$a = \sqrt{(dp/d\rho)_s}$$

was found. The Mach number $M = v/a$ was then computed, with the results presented in Fig. 32, together with M determined conventionally. Of these latter Mach numbers, only the Mach numbers for high T_0 are reliable. The variations exhibited by the calculated Mach number reflect the uncertainty of the calculation. The calculated Mach number exceeds the others in the early stages of the condensation, where the sound speed a falls as in Fig. 31. Towards the end of the expansion, the calculated M falls below the "hot" and "cold" Mach numbers.

64. Figure 12 shows that the pitot pressure is rather insensitive to changes in T_0 . The change in entropy is a process taking a perfect gas from the supply conditions (p_0, T_0) to the conditions in the pitot tube (p_0', T_0) , is

$$\Delta S = -R \ln (p_0'/p_0)$$

The pitot pressure p_0' , measured as a function of T_0 , with p_0 constant, will register ΔS , which can be called the "net irreversibility". As long as we deal with a perfect gas, regardless of condensation in the course of the process, ΔS is given by the same formula. The insensitivity of the pitot tube means that there is no marked change in "net irreversibility" due to condensation.

65. Summarizing, it can be said that:

a. The static pressure behaves about as would be expected for the isentropic expansion of a saturated vapor, at or shortly after reaching predicted equilibrium saturation conditions in the nozzle.

b. The quantity condensed is a small fraction of the flowing mass, under the operating conditions of our tunnel.

c. The ratio of (mass-average) flow speed to supply sound speed is changed little by liquefaction. The same is true for the enthalpy ratio: h/h_0' .

d. T/T_0 after liquefaction commences, no longer decreases as for perfect gas isentropic conditions.

e. p/p_0 for "hot" expansions, is nearly proportional to ρ/ρ_0 for "hot" expansions.

f. The ratio of pitot pressure to supply pressure, as a means of "net irreversibility" is insensitive to reversible condensation.

VI. LIST OF REFERENCES

- (a) Burcher, M. A. Compressible Flow Tables for Air. NACA TN No. 1592 (1948).
- (b) Dodge, B. F. and Dunbar, A. "Coexisting Liquid and Vapor Phases of Solutions of O₂ and N₂" J. Amer. Chem. Soc. 49, 591 (1927).
- ✓ (c) Wegener, P. On the experimental Investigation of Hypersonic Flow. NOLM 9629 (1948).
- (d) Bogdonoff, S. M. and Lees, L. Study of the Condensation of the Components of Air in Supersonic Wind Tunnels. Part I (Absence of Condensation and Tentative Explanation). Dept. of Aero. Eng., Princeton University Report No. 146 (1949).
- (e) Hermann, R. "Der Kondensationstoss in Ueberschallwindkanaelen", Luftfahrtforschung Bd 19 Lfg. 6, 201.
- (f) Stodola, A. Steam and Gas Turbines. McGraw Hill (1927).
- ✓ (g) Head, R. Investigation of Spontaneous Condensation Phenomena. GALCIT Dissertation (1949).
- (h) Wegener, P. "Experiments on the Influence of Temperature Gradient and Humidity on Condensation Shocks in Supersonic Wind Tunnels." Phys. Review, 76, 2nd Series, No. 6 (1949).
- (i) Cwiling, B. M. "Sublimation in a Wilson Cloud Chamber." Proc. Roy. Soc. (A), 190 (1947).
- (j) Oswatitsch, K. "Die Nebelbildung in Windkanalen und ihr Einfluss auf Modellversuche." Jahrb. Deutsch. Luftf. Forschg (1941).
- (k) Volmer, M. Kinetik der Phasenbildung. Verl. Steinkopff, Dresden and Leipzig (1939).
- (l) Becker, J. V. "Results of Recent Hypersonic and Unsteady Flow Research at the Langley Aeronautical Laboratory." Jour. of Appl. Phys., 21, No. 7 (1950).
- (m) Nagamatsu, H. J. "Results of Recent Hypersonic Flow Research in the Army Ordnance - CIT Hypersonic Wind Tunnel". Phys. Soc. Meeting, Urbane, Ill. (May 1950).

- (n) Kopal, Z. Tables of Supersonic Flow Around Cones. MIT, Dept. of Elec. Eng., Center of Analysis, Technical Report No. 1, Cambridge, Mass. (1947).
- (o) Moeckel, W. E. and Connors, J. F. Charts for the Determination of Supersonic Air Flow Against Inclined Planes and Axially Symmetric Cones. NACA TN No. 1373 (1947).
- (p) Kurzweg, H. The Pressure on the Base of Bodies at Supersonic Speeds. NOLM 9609 (1948).
- (q) Faro, I.D.V., Small, T. R. and Hill, F. K. Flow at a Mach Number of 10. APL/JHU CM-604 (1950).
- (r) van de Hulst, H. C. Optics of Spherical Particles. J. F. Duwaer and Conen, Amsterdam (1946).
- (s) Haybey, W. Analytical Treatment of Normal Condensation Shocks. WVA Archive 65/72, (1942). Translation by Cornell Aero. Lab. CGD 322, (1946).
- ✓(t) Wegener, P. and Smelt, R. Summary of NOL Research on Liquefaction Phenomena in Hypersonic Wind Tunnel. NOLM 10772 (1950).
- (u) Buhler, R. Recent Results on the Condensation Investigation. GALCIT Memorandum (July 1950).
- (v) Bosnjakovic, F. Technische Thermodynamik, volume I and II, Steinkopf, Leipzig (1944).
- (w) Vonnegut, B., Continuous Recording Condensation Nuclei Meter, Occasional Report No. 19, Project Cirrus, Rep. R.L.-300, G.E. Jan. 1950.

APPENDIX I

Thermodynamic Analysis of Condensation Process

Consider a reversible adiabatic expansion of a single-component vapor which proceeds beyond the point of condensation (reference f). If this vapor, expands reversibly in an adiabatic enclosure, its entropy is constant. Beyond the "dew-point", the total entropy S of the two phases, vapor and condensed, will still have the same constant value,

$$S = S_o = S_c + S_v \quad , \quad (1)$$

where S_v is the entropy of the vapor and S_c is the entropy of the condensed phase. Referred to one gram of the mixture, this can be expressed as

$$s = S_o = g s_c + (1-g) s_v \quad (2)$$

where the small s refers to entropy per gram, and

$$g = \frac{(\text{mass condensed})}{(\text{unit mass of mixture})} = T \frac{s_v - s_o}{L} \quad (3)$$

where T is temperature and L is the latent heat per gram. To obtain g , a knowledge of the entropy of the vapor phase and of the latent heat is sufficient. There is a relation between the temperature T and the vapor pressure p , given by the vapor pressure equation $T = \varphi(p)$, so that pressure data for the isentropic expansion, together with knowledge of latent heat are enough to determine g .

The vapor can be taken to be a perfect gas. Then we can write

$$p = \rho_v R_v T \quad (4)$$

where ρ_v is the vapor density, and R_v is the gas constant per gram of the vapor. The mixture density ρ is related to ρ_v and the density of condensed phase ρ_c by:

$$\frac{1}{\rho} = \frac{g}{\rho_v} + \frac{(1-g)}{\rho_c} \quad (5)$$

The first term on the right-hand side can be neglected in comparison with the second, so that $\rho_v \cong \rho(1-g)$ and

$$p = \rho(1-g) R_v T \quad (6)$$

i.e.
$$\rho = \frac{p}{(1-g)R_g T} = \frac{p}{(1-g)R_g \varphi(p)} \quad (7)$$

The pressure p can be plotted against ρ , and the slope of the curve $a^2 = dp/d\rho$ found. (See Fig. 30).

To apply the above concepts, we assume the expansion in the nozzle is steady and one-dimensional.

The rate of expansion is controlled by the cross-section area A , which is a function of length x along the nozzle centerline, measured from the throat.

The equation of motion can be written in the form:

$$\rho v \frac{dv}{dx} = - \frac{dp}{dx} \quad (8)$$

or
$$\frac{1}{2} \frac{dv^2}{dx} = - v \frac{dp}{dx} \quad (9)$$

where v is the average-mass flow speed, ρ is the mixture-density, and $v = \rho^{-1}$ the specific volume.

The expansion follows ODE in Fig. 30. At D there will be a jump in dp/dv , as well as in dp/dx and in dv^2/dx .

In fact

$$\frac{dv^2/dx}{dv^2/dx} = - \frac{dp/dv}{dp/dv} \quad \text{and} \quad dv^2/dx = a^2 \frac{d \ln v^2}{dx}$$

and, as in Fig. 32, a decreases sharply at D.

If the pressure p is known for a saturated expansion as a function of x , ρ can be found from equation (7). Then, if the value of the flow speed is known at one point along the nozzle, the speed at the other points may be found by integrating equation (9) to give

$$v(x) = \left(v_1^2 + \frac{1}{2} \int_1^x \frac{dp}{\rho} \right)^{1/2} \quad (10)$$

Finally
$$M = \frac{v}{a} \quad (11)$$

can be found for each point along the nozzle.

The overall continuity equation for the mixed flow (vapor plus liquid phase) is

$$\rho v A = \text{const.} \quad (12)$$

so that, were p measured along the nozzle, A could now be computed. Conversely, were A known, and not p , all the necessary information could be obtained. A and p are not independent, under the hypothesis of an isentropic saturated expansion.

We now assume both phases have the same flow speed. Then, the energy equation for the mixed-flow isentrope reads

$$v dv + dh = 0 \quad (13)$$

where h is the specific enthalpy of the mixture, given by

$$h = g h_c + (1-g) h_v \quad (14)$$

or

$$h = C_p T - g L \quad (15)$$

Hence h_c is the specific enthalpy of the condensed phase, h_v that of the vapor phase, L , as before, latent heat of vaporization, and C_{pv} the specific heat per gram of the vapor. C_{pv} may be considered constant, L may be expected to be nearly constant, at the low temperatures of interest here.

In the experiments described in this report the expanding vapor was air, which is approximately a binary mixture of N_2 and O_2 , rather than a single component substance. The dewpoint line of air has not been determined experimentally. It could be calculated, however, from a knowledge of the vapor pressure.

The vapor pressure and latent heat of air depend on the equilibrium composition, (see, e.g., reference (v)). None of these has been measured in the range of pressures and temperatures of interest here. The principal measurements of vapor pressures and composition (reference b) go down to only 1/2 atm pressure and about 77 degrees K.

In the work reported here, air was treated as a fictitious single-component substance having vapor pressures obtained by extrapolating the data of reference (b).

The equations of continuity and momentum, (8) and (12), give in dimensionless form

$$\int_1^x \frac{d}{dx} \left(\frac{v}{a_0} \right) dx = -b \int_1^x \left(\frac{A}{A^*} \frac{d}{dx} \left(\frac{p}{p_0} \right) \right) dx \quad (16)$$

where $a_0 = \sqrt{\gamma R T_0}$ is the sound speed at supply temperature, p_0 is the supply pressure, A/A^* is the ratio effective area/throat area, and b is a numerical constant of order 1.

The first point to be noted is that v/a , for our two operating conditions, "hot" and "cold", will be equal to within a few percent. The argument for this is as follows:

Equation (16) applies to both "hot" and "cold" runs. Writing (16) explicitly for these two conditions, distinguished by subscripts 1 and 2, we have that

$$\int_1^x \frac{d}{dx} \left(\frac{v_1}{a_{01}} \right) dx = -b \int_1^x \frac{A_1}{A_1^*} \frac{d}{dx} \left(\frac{p_{01}}{\rho_{01}} \right) dx \quad (16a)$$

$$\int_1^x \frac{d}{dx} \left(\frac{v_2}{a_{02}} \right) dx = -b \int_1^x \frac{A_2}{A_2^*} \frac{d}{dx} \left(\frac{p_{02}}{\rho_{02}} \right) dx \quad (16b)$$

If we take common limits of integration, one upstream of the dew-point, where p/p_0 and v/a_0 have the same values, for both "hot" and "cold" runs and the other at the nozzle exit, and subtract (16b) from (16a) we obtain

$$\left(\frac{v_1}{a_{01}} - \frac{v_2}{a_{02}} \right)_E = -b \left\{ \int_1^E \frac{A_1}{A_1^*} \frac{d}{dx} \left(\frac{p_{01}}{\rho_{01}} \right) dx - \int_1^E \frac{A_2}{A_2^*} \frac{d}{dx} \left(\frac{p_{02}}{\rho_{02}} \right) dx \right\}$$

where E refers to the coordinate of the nozzle exit. If we call (A/A^*) the maximum of the two quantities A_1/A_1^* and A_2/A_2^* , and take absolute values of both sides, one has

$$\left| \frac{v_1}{a_{01}} - \frac{v_2}{a_{02}} \right|_E \leq |b| \cdot \left| \frac{A}{A^*} \left(\frac{p_{01}}{\rho_{01}} - \frac{p_{02}}{\rho_{02}} \right)_E \right|$$

Numerically, the difference $\left| \frac{p_{01}}{\rho_{01}} - \frac{p_{02}}{\rho_{02}} \right|_E$ is experimentally of order $2 \cdot 10^{-4}$ (see Fig. 11), and for Mach numbers ≤ 8 , $A/A^* \leq 200$. Remembering that $|b| \cong 1$, we have $\left| \frac{v_1}{a_{01}} - \frac{v_2}{a_{02}} \right|_E < 4 \cdot 10^{-2}$. Since $|v/a_0| \cong 2$, this means that v/a values for "hot" and "cold" runs differ by less than 2 percent under our operating conditions.

A similar integration of the energy equation (13) is possible. For a perfect gas the total (supply) enthalpy h_0 is given by

$$h_0 = C_p T_0 = \frac{a_0^2}{\gamma - 1}$$

Integrating (13) between supply conditions and the nozzle exit, gives

$$\left(\frac{v^2}{a_0^2} \right)_E = \frac{h_0 - h_E}{(\gamma - 1) h_0} = \frac{1}{\gamma - 1} (1 - h_E/h_0) \quad (17)$$

Then the fact that v^2/a_0^2 does not change by more than 4 percent between the extremes of supply temperature implies that

$$\frac{1}{\gamma - 1} (1 - h_E/h_0)$$

also does not change by more than 4 percent between these extremes. As long as γ can be considered nearly constant, it follows that h_E/h_0 is nearly independent of T_0 over the range from "hot" to "cold".

The equation of continuity (12) applied to both "hot" and "cold" expansions, designated by subscripts 1 and 2, gives

$$\frac{\rho_1 v_1}{\rho_{01} a_{01}} A_1 = \frac{\rho_2 v_2}{\rho_{02} a_{02}} A_2 \quad (18)$$

and since $v_1/a_{01} \cong v_2/a_{02}$,

$$\text{also } \rho_1/\rho_{01} = \frac{A_2}{A_1} \cdot \frac{\rho_2}{\rho_{02}} \quad (19)$$

The quantity g was computed by two methods, with fairly consistent results. In the first method, area ratios obtained from the measured pressures for "hot" expansions, which were assumed isentropic, were used as a first approximation to the area ratios of the "cold" expansions. To this approximation values of ρ/ρ_0 are independent of T_0 . The values for g found in this way are shown in Fig. 33.

The other, more direct method was to use equation (3) with the static pressure data and extrapolated vapor-pressure data. These values of g were in fair agreement with those shown in Fig. 32.

For a saturated one-dimensional isentropic expansion the effective area can be computed from pressure measurements along the nozzle. The consistency of taking the area from the "hot" assumed isentrope for the effective area of the saturated expansion can therefore be tested. An accurate calculation of A from the assumption of a saturated expansion depends again on the accuracy of vapor pressure data. We checked only the consistency of values of A obtained from the assumed vapor pressures and latent heats. The agreement of these values of A is rather poor. Consequently agreement of densities, computed by using equation (19) in the first method (equal A), with those found using equation (7) in the second method, was also rather poor.

However, when p - ρ graphs were drawn using observed pressures and the two different values of density, the slopes $dp/d\rho$ evaluated at the same value of x for the two curves were in fair agreement. Then it was possible to assign unambiguously a value of $dp/d\rho$ and so of Mach number $M = v/a$ for the expansions. The values of M thus obtained are exhibited in Fig. 33 and have been discussed already.

APPENDIX II

Design and Operation of The NOL 12 x 12 cm Hyperballistics Tunnel No. 4

A. Design

The 12 x 12 cm Hyperballistics Tunnel No. 4 has a vertical test section. Figure 1 shows a view of the tunnel and its components. Figure 2 gives a schematic layout. Atmospheric air dried in a silica gel filter enters two Norwalk, 50 horsepower, reciprocating compressors. The compressors discharge the air at about 3000 psi via two 25 cubic feet oil settling tanks, and a lectrofilter to free the air of oil vapor. The filling of the filter is activated alumina. The air then passes through two Pittsburgh-Lectodryer-Dehumidifiers into twenty-one high-pressure air storage tanks. The total storage volume is 525 cubic feet, at 3000 psi.

A four-inch and a one-inch Hammel-Dahl high-pressure reducing-regulator valve reduces the high pressure air to a desired pressure, discharging it into the settling-chamber of the wind tunnel. The regulators are single-seated valves with a plug design of linear characteristics. The percentage of maximum plug lift when plotted against the percentage of maximum flow is found to vary linearly. A Taylor-Fulscope pressure-recording controller regulates the stroke of the high-pressure reducing regulator valves in such a way that the supply pressure of the tunnel is held constant to about 1% at any desired value from 15 to 900 psi.

The air passes through a heater in the settling tank. This heater consists of edge-wound nichrome units, and has a total installed capacity of 80 KW. For heating requirements above 40 KW, a load of 40 KW is connected continuously. Control is maintained by means of a Leeds and Northrup proportional heat controller, which controls contactors that cut-out the remaining 40 KW periodically as needed to maintain the temperature of the air. The heater controls are set to give a temperature within one percent of the desired value.

For heating requirements below 40 KW, the 40 KW continuous load is switched off. The control is then maintained by "cutting" in and out the remaining 40 KW. This type of control proved to be satisfactory since the heater as a whole has a relatively large heat-capacity. The heater is also provided with a Wheeler over-temperature protector.

At high Mach numbers, ranging from 7 and up, the velocity of the air through the heater is approximately one-half foot per second, or less; therefore, a "by-pass" is used to permit increased velocity through the heater.

The air leaving the heater is passed through a filter of 0.0065 mesh. The air leaving the settling-tank passes through a fast-acting, high-pressure

slide valve. This valve is used to start and stop the flow of air. The air then passes through the test section into a simple adjustable diffuser and a 12" gate valve. Finally it is discharged into a 2000 cubic meter vacuum tank exhausted by 6 rotary vane type vacuum pumps. (1000 HP).

At present the tunnel is equipped with two sets of parallel flow nozzles for $M = 1.86$ and 5.18 . Also a simple wedge nozzle to cover a Mach range from approximately 4 to closure of the throat is available. Figure 3 shows the working section. All nozzles are solid aluminum blocks, bolted and pinned to a standard baseplate. The baseplate itself has three adjustable supporting legs to permit proper initial setting of the nozzle halves with respect to each other. In the case of the wedge nozzle this adjustment is used to set the proper area ratios for the desired Mach number.

The interchangeable nozzles are held in position by a heavy lever. When a nozzle is inserted into the tunnel it is manually placed in its approximate position and one end of the lever is engaged with the nozzle baseplate by insertion of a pin. The other end of the lever is moved by a jackscrew until the nozzle is seated. Lateral alignment of the nozzle in the tunnel is determined by two pins which protrude from the bottom of the baseplate engaging slots in the nozzle bed. Tightening the jackscrew accomplishes two functions. It forces the nozzle to move until the upstream end of the nozzle baseplate butts against a shoulder of the test section housing and assures the final location of the nozzle in flow direction. Simultaneously the legs are forced against their seating area. This assures proper separation of the two nozzle halves. Exchanging nozzles requires about 10 minutes.

The diffuser consists of one pair of moveable straight plates having a length of about 11". The cross-sectional area of the diffuser entrance can be adjusted during the run from 90% - 125% of the final cross-sectional area of the nozzle, (12 x 12 cm). Its location is 8 inches aft of the nozzle exit. The tunnel can be operated as a closed or half-open jet. This is accomplished by two removable jet plates.

Two doors form the parallel side walls of the tunnel. The following doors are available:

One pair with glass covering the entire flow channel; one pair with interchangeable glass or steel panels; (by inverting each entire rectangular frame visibility coverage of the complete working section is possible), one pair of steel doors.

Forty durometer silicone rubber, which was selected for high temperature resistance, has been used as gasket material on sidewalls, nozzles and diffuser.

A heavy rubber diaphragm is used to connect the 12" diameter gate valve to the 36" diameter vacuum header pipe from the vacuum sphere. Since the entire tunnel is suspended from the ceiling, this diaphragm permits movement of the tunnel due to thermal expansion, and provides vibration isolation from the vacuum sphere and pumps.

The settling tank is provided with a lead-off pipe to the outside of the building where it is capped by a dome-shaped beryllium bronze rupture diaphragm which will be punctured by a pre-set mechanism if the working supply pressure is exceeded. If, for any emergency, it is desired to jettison the pressure in the settling tank, the rupture diaphragm can be punctured electrically or mechanically at any time. The test section is provided with a blow-off valve which will discharge any pressure in excess of atmospheric pressure.

B. Operation

The 12 x 12 cm hyperballistics wind tunnel is of the continuous non-return type. Since the vacuum capacity of the "suction side" is larger than required, the duration of blow depends on the capacity of the high pressure air tanks. This supply is regarded as continuous (order of hours) in the range 5 M_{all}.

The tunnel operating procedure is as follows: Select nozzle desired. In case of wedge nozzle select desired area ratio. Set diffuser on minimum area required for starting at given Mach number. Align instruments or models and close and secure doors. Pump vacuum sphere to desired pressure. Open 12" gate valve and connect test section to vacuum with closed slide valve. Set pressure controller to desired supply pressure. When this pressure is built up in settling tank, flow to tank is shut off automatically. Set temperature controller to desired supply temperature and operate by-pass. If T_0 and p_0 are attained, start tunnel by opening fast-acting slide valve. If supersonic flow is established, close diffuser to optimum running throat area.

APPENDIX III

Instrumentation

Some of the probes and models in use can be seen in Fig. 34. Both wedges and cones with angles of 10° , 40° , 80° , and 120° are shown. Each wedge and cone has a pressure tap near its base for the measurement of base pressure. The 10° wedge has a pressure tap on each face for the measurement of flow direction and pressure coefficient.

Conventional pitot probes are made from steel hypodermic tubing,¹ (Superscripts refer to list of manufacturers, Table IV at end of Appendix III.) having an inside diameter of .063". This tubing is held in the tunnel with small holders mounted to the test section wall. It extends from the point at which the pressure is to be measured through the diffuser and out through an opening in the 12" pipe near the floor (see Fig. 2), where it is connected to a manometer. This arrangement eliminates the difficulty of making tight hose connections at high temperatures inside the wind tunnel.

For pitot surveys across the test section at the nozzle exit a probe made from hypodermic tubing and a right angle fitting, is employed. This probe can be moved electrically across the air stream. In addition to the single pitot probe, a three tube pitot rake can be mounted in the same fashion. The three separate pitot tubes on this rake are mounted $1 \frac{3}{16}$ inches apart on a biconvex strut. This rake is useful for determining the boundary layer thickness at the nozzle wall.

Two types of static centerline probes are used. A large probe is shown at A in Fig. 4. It is a 10° cone-cylinder probe with three static pressure holes in the cylinder wall.

The smaller probe is constructed from hypodermic tubing .108 inches in diameter which has been filled at the head and filed to a point. There are four holes 90 degrees apart $3 \frac{3}{4}$ inches back from the probe tip. These holes all lead into the hollow center of the hypodermic tubing.

Wall static pressures can be taken by replacing one of the observation doors with a solid door which has pressure taps every inch along the centerline for the entire length of the wind tunnel. These pressure holes are 0.031. Duplicate sets of hinges to hold the doors are provided on both ends of the tunnel so that the doors may also be hung upside down. When in this position, each hole is displaced $1/2$ inch from its previous position.

All test pressures are measured with either mercury, oil, or McLeod manometers.

For measuring pressures below 20 millimeters, oil manometers are used. A number of butyl phthalate manometers² are available. A small manometer using silicone oil is also used. A bank of silicone oil manometers to indicate pressures up to 100 millimeters mercury is being completed. All of the oil manometers operate with a high vacuum reference pressure which is obtained with a small mechanical and diffusion pump combination. It is held below 5 microns pressure and monitored with a Phillips ionization type pressure gage.² An accuracy of $\pm .02$ millimeters of mercury is attainable with pressure measurements on any of these manometers.

Two types of McLeod gages are occasionally used for accurate measurement of very low test pressures also, although their suitability for this is limited by their large volume and slow response.

Supply pressures are measured just above the nozzle throat with a total head probe³ connected to a Heise Bourdon-type gage⁴ having a range of 0-150 psi (for the tests described in this report). This gage is calibrated with a dead weight tester⁵.

Vacuum sphere pressure is measured with aneroid type absolute pressure gages⁶.

All pressures can also be electrically measured and recorded. This is accomplished with an Alphatron radium source ionization gage⁷ for pressures in the ranges 0-.1,⁸ and 0-1, and 0-10 millimeters of mercury, and with Statham strain gages⁸ for all other pressures up to 1000 psi.

The supply temperature is measured with iron-constantan thermocouple^{9,3} placed in approximately the same position as the supply pressure probe. They are connected to one of two high speed potentiometer recorders⁹ covering temperature gages of 0-300 or 0-600 degrees Centigrade. The accuracy of the temperature measurements with the present set-up is ± 2 degrees Centigrade.

A Pyrocon¹⁰ portable thermocouple and indicator is used for spot safety checks of the temperature of tunnel and heater walls. It indicates temperatures up to 800°F when touched to the surface to be tested.

The water vapor content of the supply air is determined with a dew-point indicator¹¹. The small flow of supply air needed in the indicator is throttled through a needle valve from the wind tunnel settling tank and passed through copper tubing to the instrument. At the low dew-point of about -50°F or better, the accuracy is only about $\pm 5^\circ\text{F}$.

High pressure dew-point indicators¹² have been procured which will be mounted at different points in the high pressure system so that spot checks of humidity can be made at various locations. An electric hydrometer¹³

will also be mounted in the tunnel supply tank for continuous indication or recording of supply humidity.

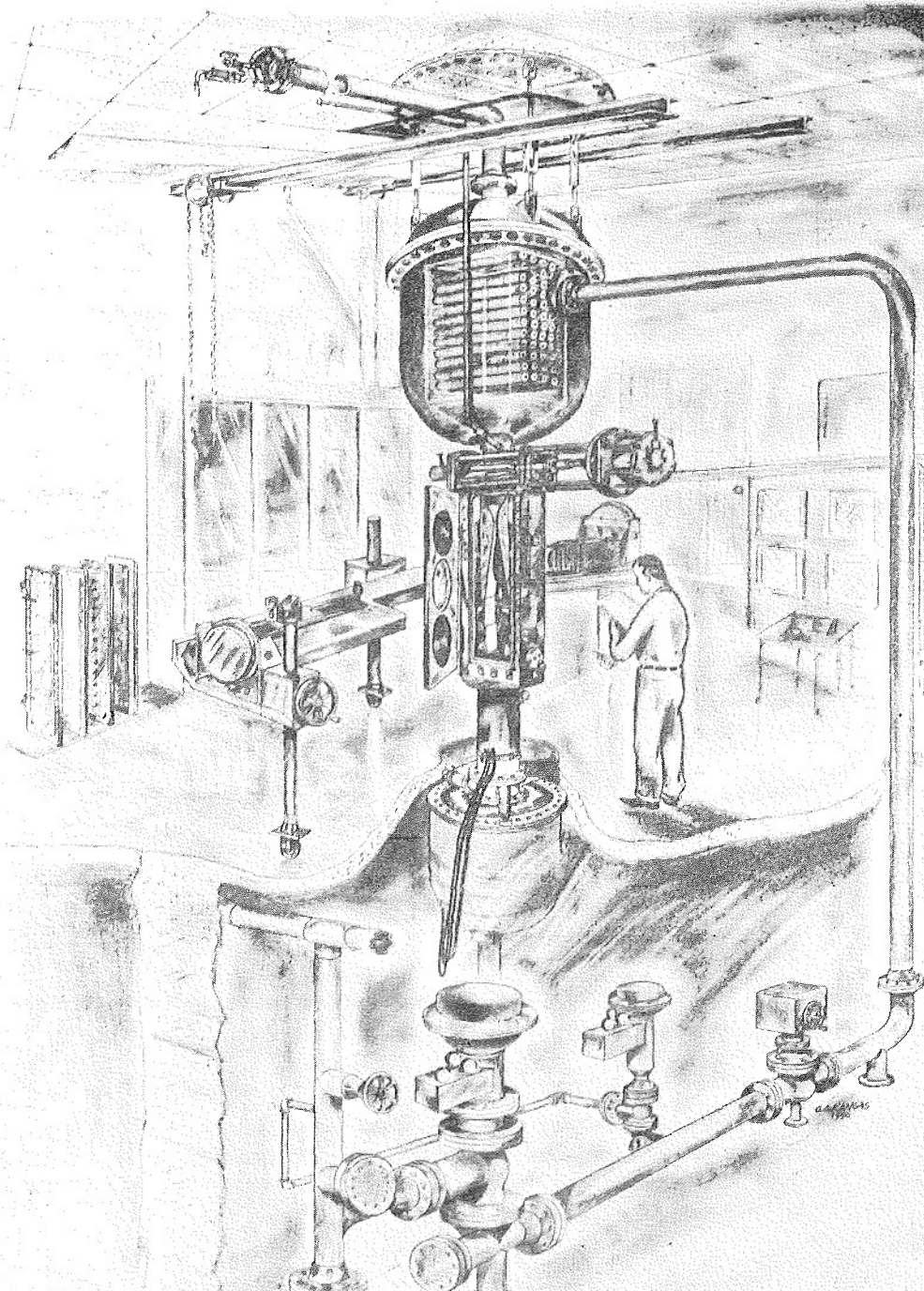
An instrument which will continuously indicate and record the concentration of condensation nuclei in the wind tunnel supply air has been built for use in conjunction with the condensation program. It is patterned after one developed by the General Electric Research Laboratory for the Project Cirrus (reference w).

The wind tunnel is equipped with shadowgraph and schlieren systems. The schlieren system is a standard double mirror system integrally mounted on a movable optical bench (Fig. 1). Light sources in use are a 300 watt zirconium arc¹⁴ which furnishes a steady, concentrated, white light, a 1000 watt zirconium arc¹⁴ source when more intense light is needed, and a high pressure mercury vapor light source¹¹. This last source can be made monochromatic if desired, and it can be flashed to give exposures of a few microseconds for studying transient phenomena. For flashing, a 10 kilovolt power supply is used to charge a condenser, and this is then discharged through the mercury vapor tube with a mercury switch or a thyratron. A more intense light with exposures of one microsecond or less can be obtained from a 15 kilovolt Liebessart type spark. In it, a .12 microfarad condenser charged to 15 kilovolts, is discharged through a confined gap to produce very intense light with extremely short duration.

TABLE III
List of Manufacturers

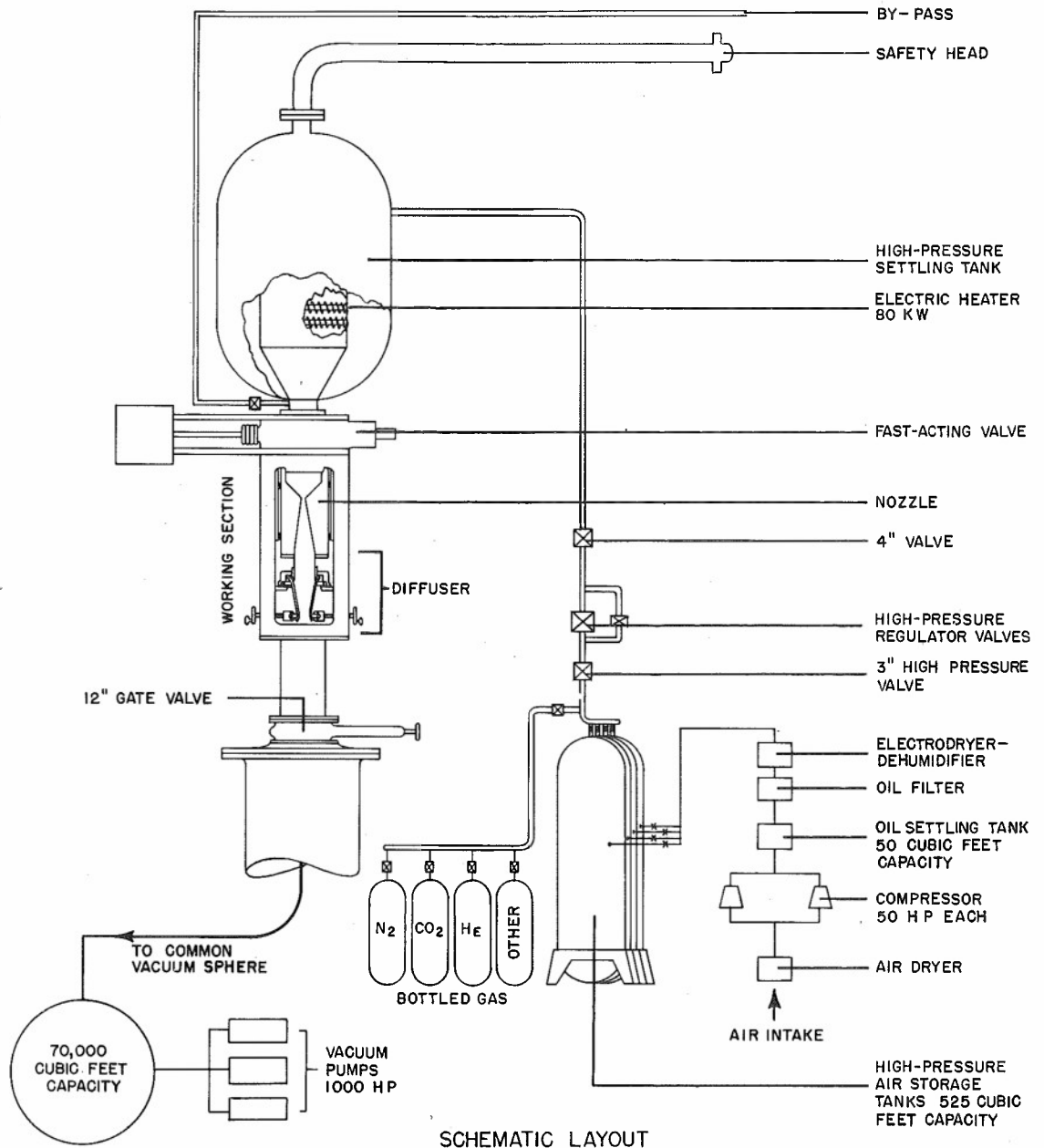
1. Illinois Surgical Supply Co.
10 S. Wells St., Chicago, Ill.
2. Distillation Products Company
Vacuum Equipment Division, Rochester 13, N. Y.
3. Revere Corporation of America
Wallingford, Connecticut
4. Heise Bourdon Tube Co., Inc.
Brook Road, Newtown, Conn.
5. Coleman Instrument Company
716 S. Troost St., Tulsa, 5, Okla.
6. Wallace and Tiernan Products, Inc.
Belleville, 9, N. J.
7. Vacuum Engineering Division, National Research Corp.
Cambridge, 42, Mass.
8. Statham Laboratories, Inc.
9328 Santa Monica Blvd., Beverly Hills, Calif.

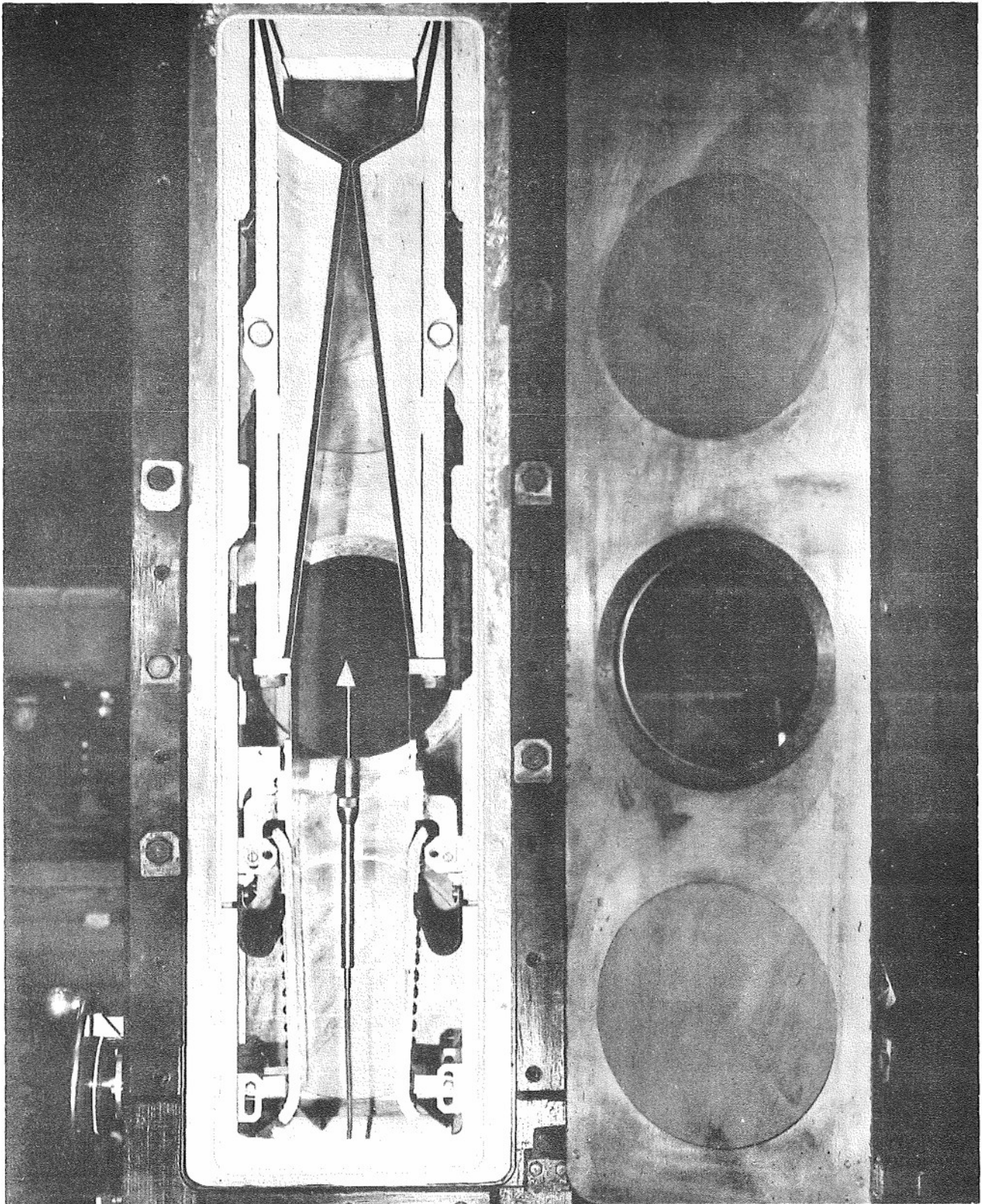
9. The Brown Instrument Company
Philadelphia, 44, Pa.
10. Illinois Testing Laboratory, Inc.
420 N. LaSalle St., Chicago, 10, Ill.
11. General Electric Company
Schenectady, New York
12. Refinery Supply Company
621 E. 4th Street, Tulsa, 3, Okla.
13. American Instrument Company
8010 Georgia Avenue, Silver Spring, Md.
14. Western Union Telegraph Company, Electronics Research Lab.
Water Mill, Long Island, New York



12x12 cm HYPERBALLISTICS TUNNEL N°4
NAVAL ORDNANCE LABORATORY-WHITE OAK, MD

FIG. 2





NOL 12 X 12 CM HYPERBALLISTICS TUNNEL NO.4
TEST SECTION

FIG.4

$$M = f(\ell/W)$$

○ = ONE-DIMENSIONAL THEORY, M FROM AREA RATIO

□ = TWO-DIMENSIONAL THEORY, M ON CENTER LINE
FROM METHOD OF CHARACTERISTICS

ℓ - DISTANCE FROM THROAT

W - WIDTH OF NOZZLE AT ℓ

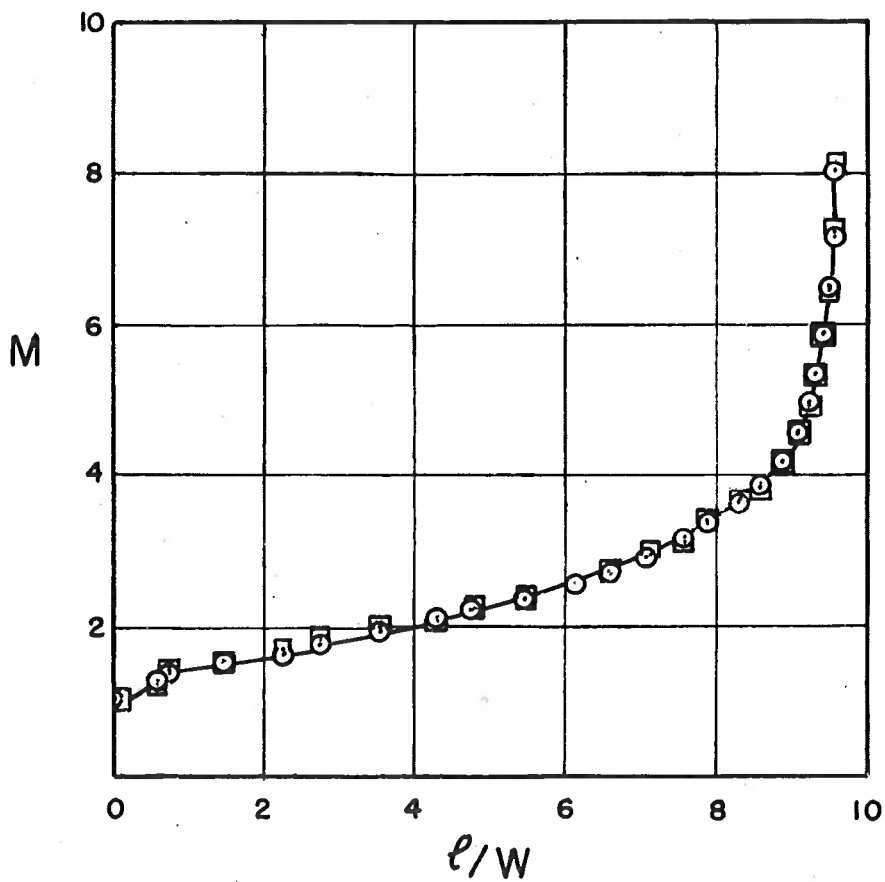
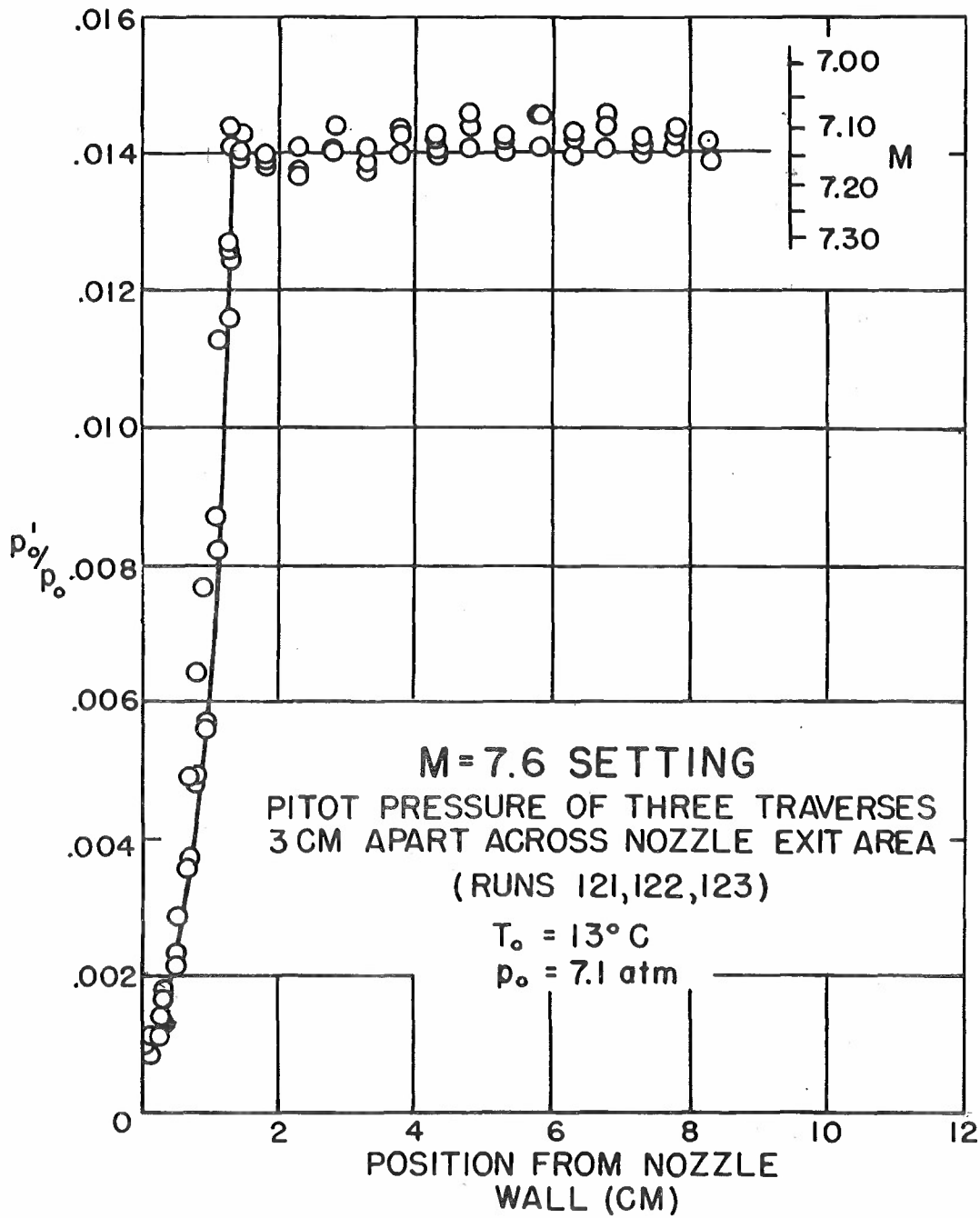
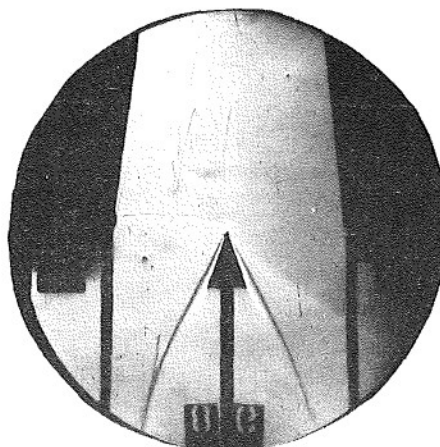
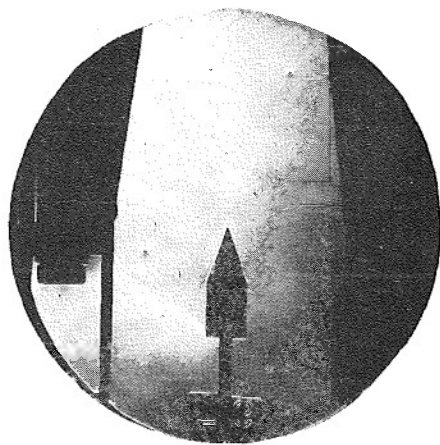


FIG. 5

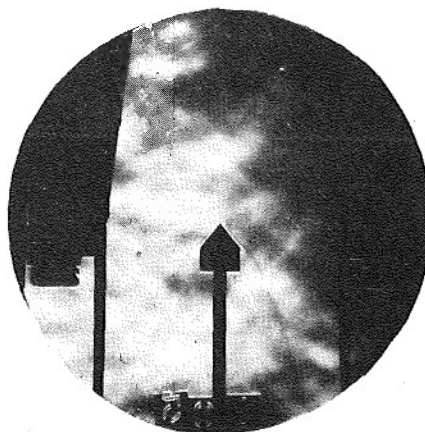




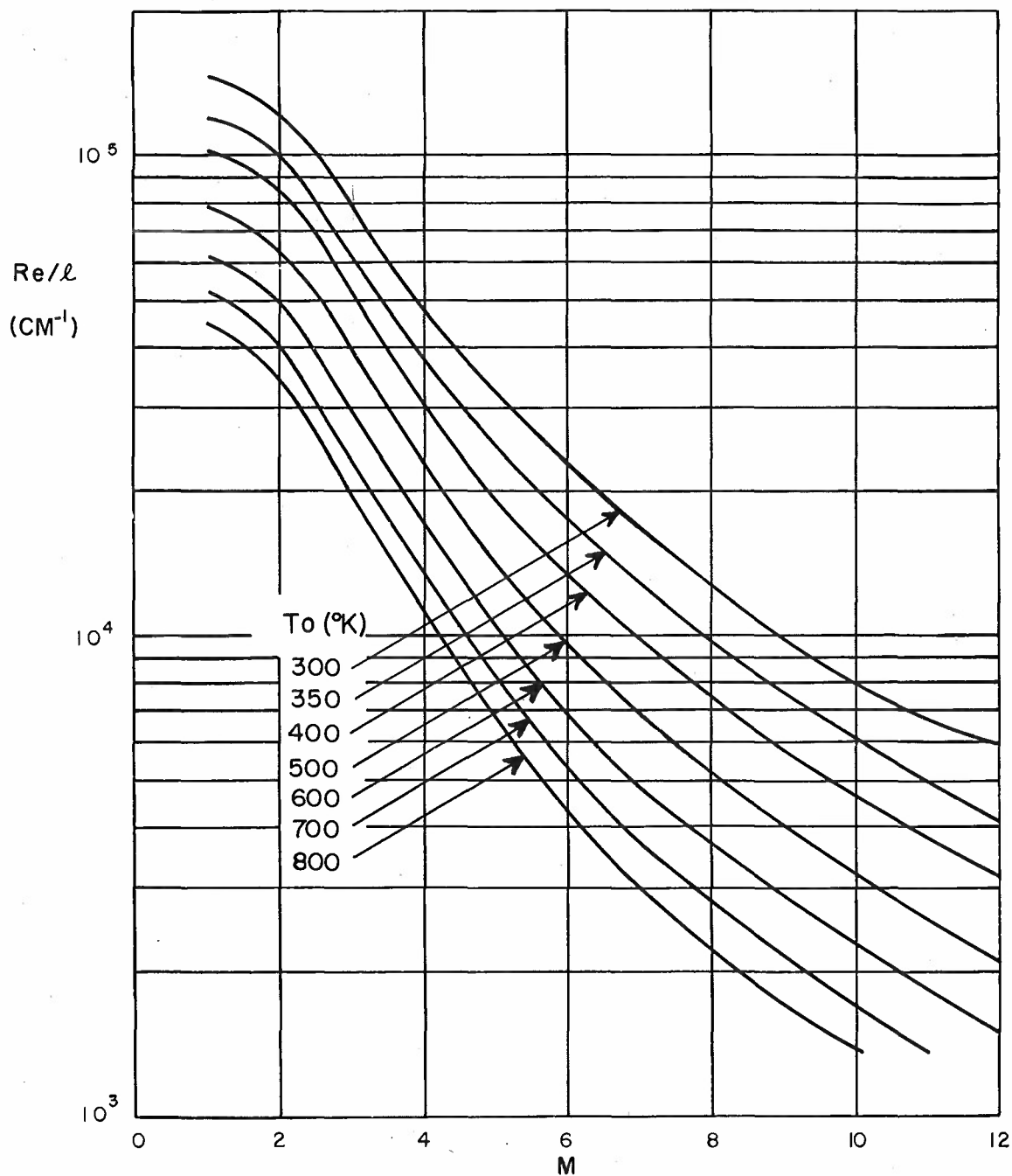
40° WEDGE, $T_0 = 121^\circ\text{C}$



40° CONE, $T_0 = 116^\circ\text{C}$



80° CONE, $T_0 = 93^\circ\text{C}$

REYNOLDS NUMBER BASED ON VISCOSITY
FROM SUTHERLAND'S FORMULA WITH $C=120$ $P_0 = 1 \text{ ATM}$ 

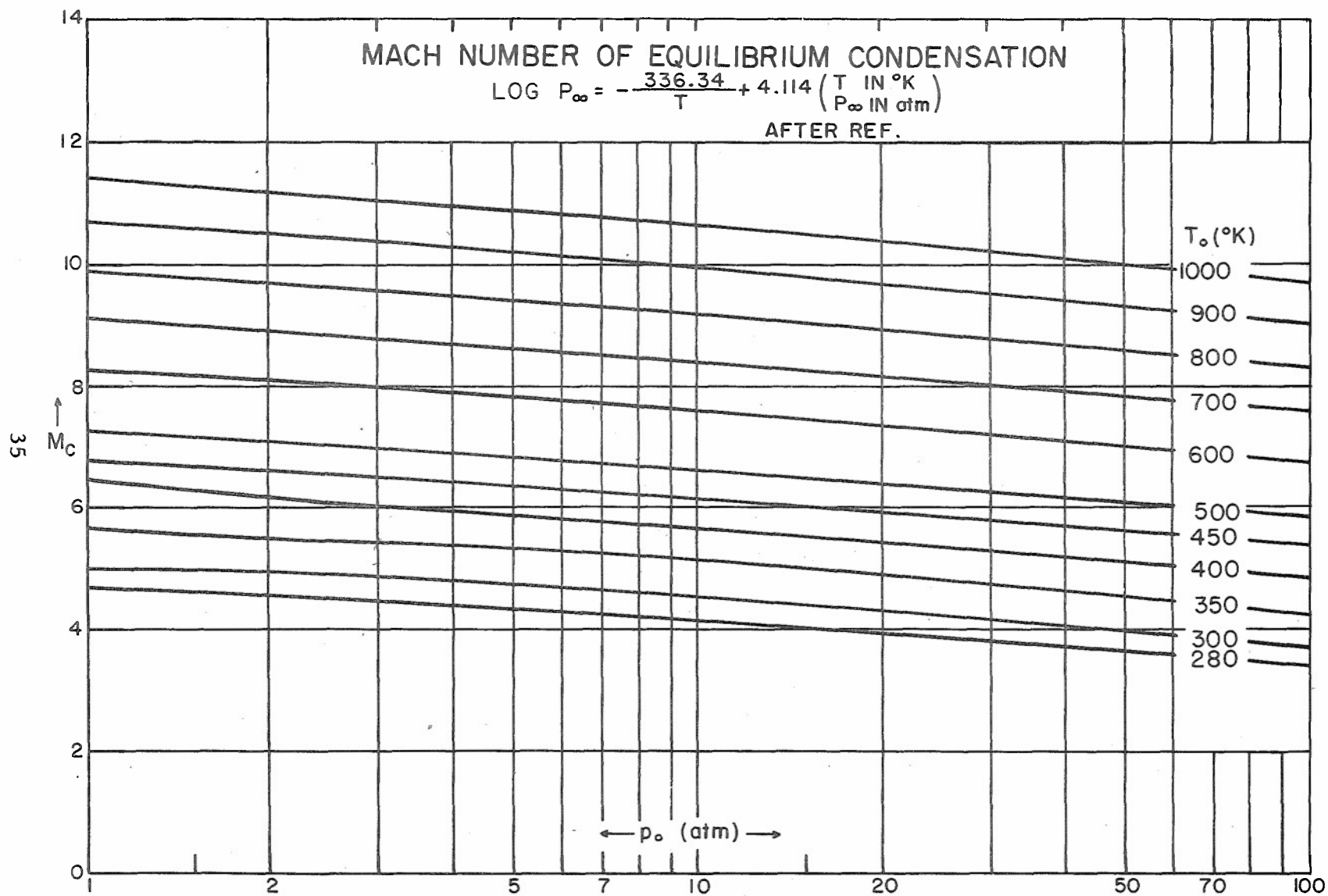


FIG. 8

FIG. 9

M = 6 SETTING

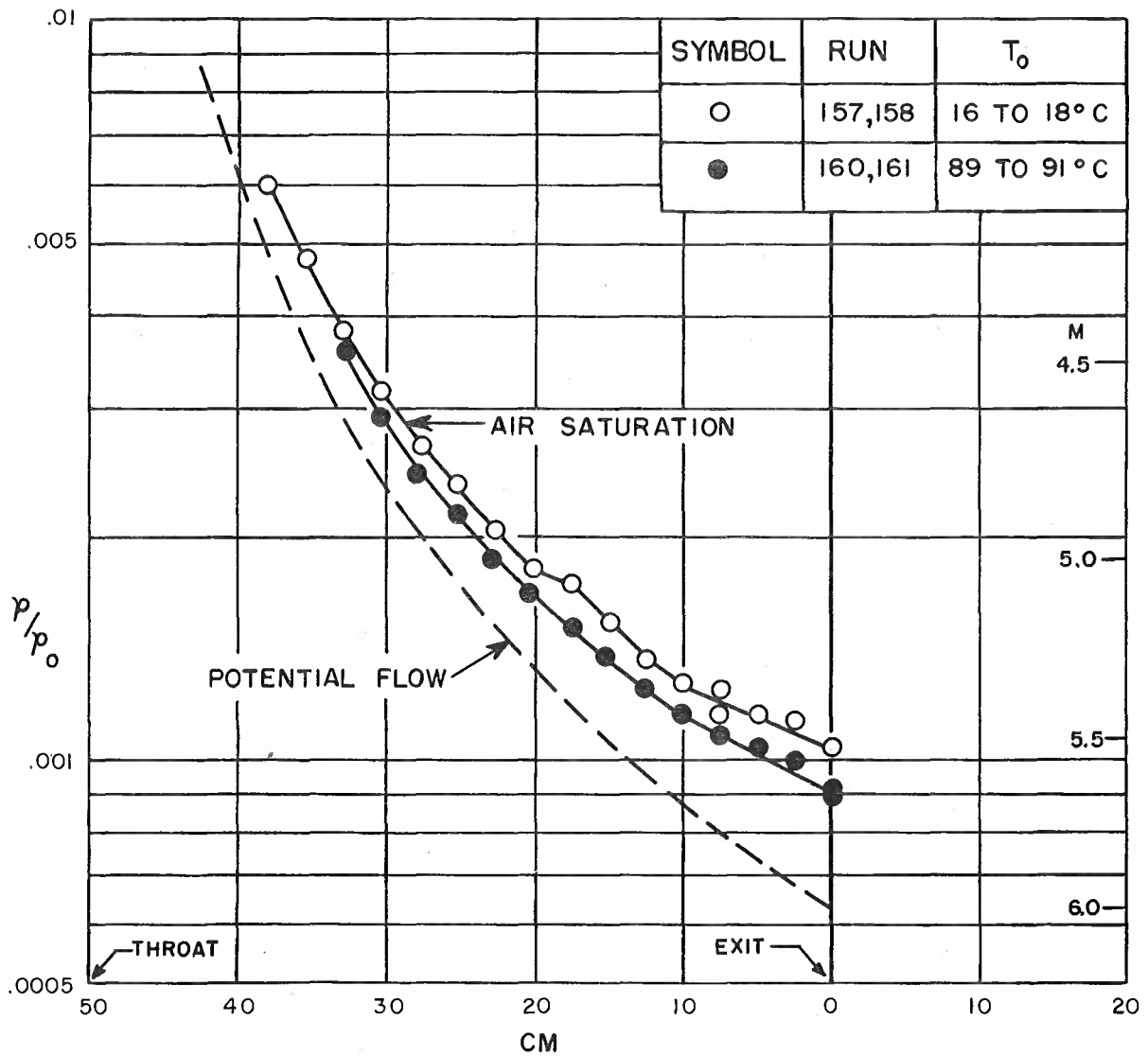
 $P_0 = 3.04 \text{ ATM}$ 

FIG. 10

M = 7 SETTING

STATIC PRESSURE ON WALL CENTER LINE

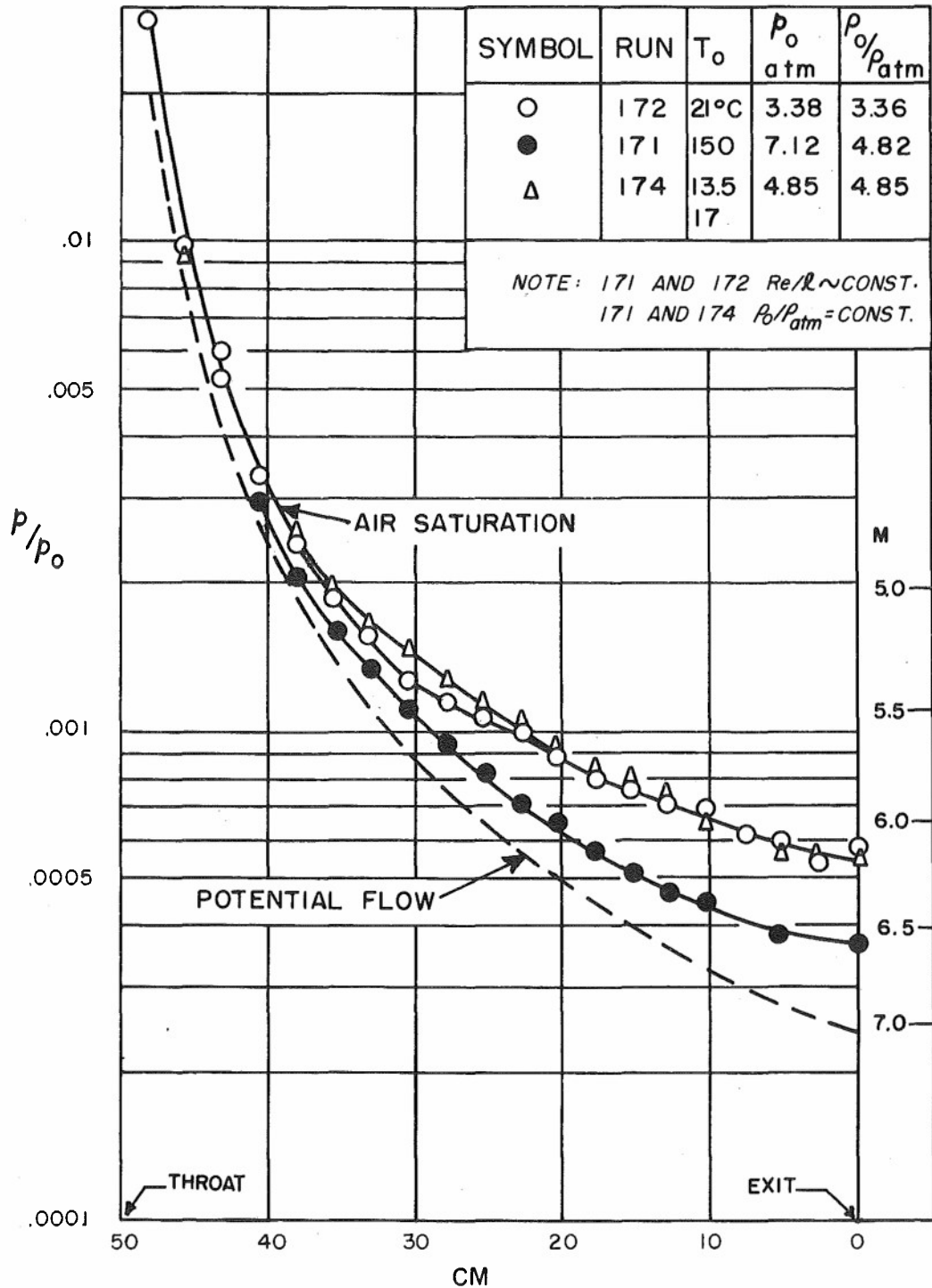


FIG.11

M = 7.6 SETTING
 STATIC PRESSURE ON WALL CENTER LINE
 $p_0 = 7.1$ ATM

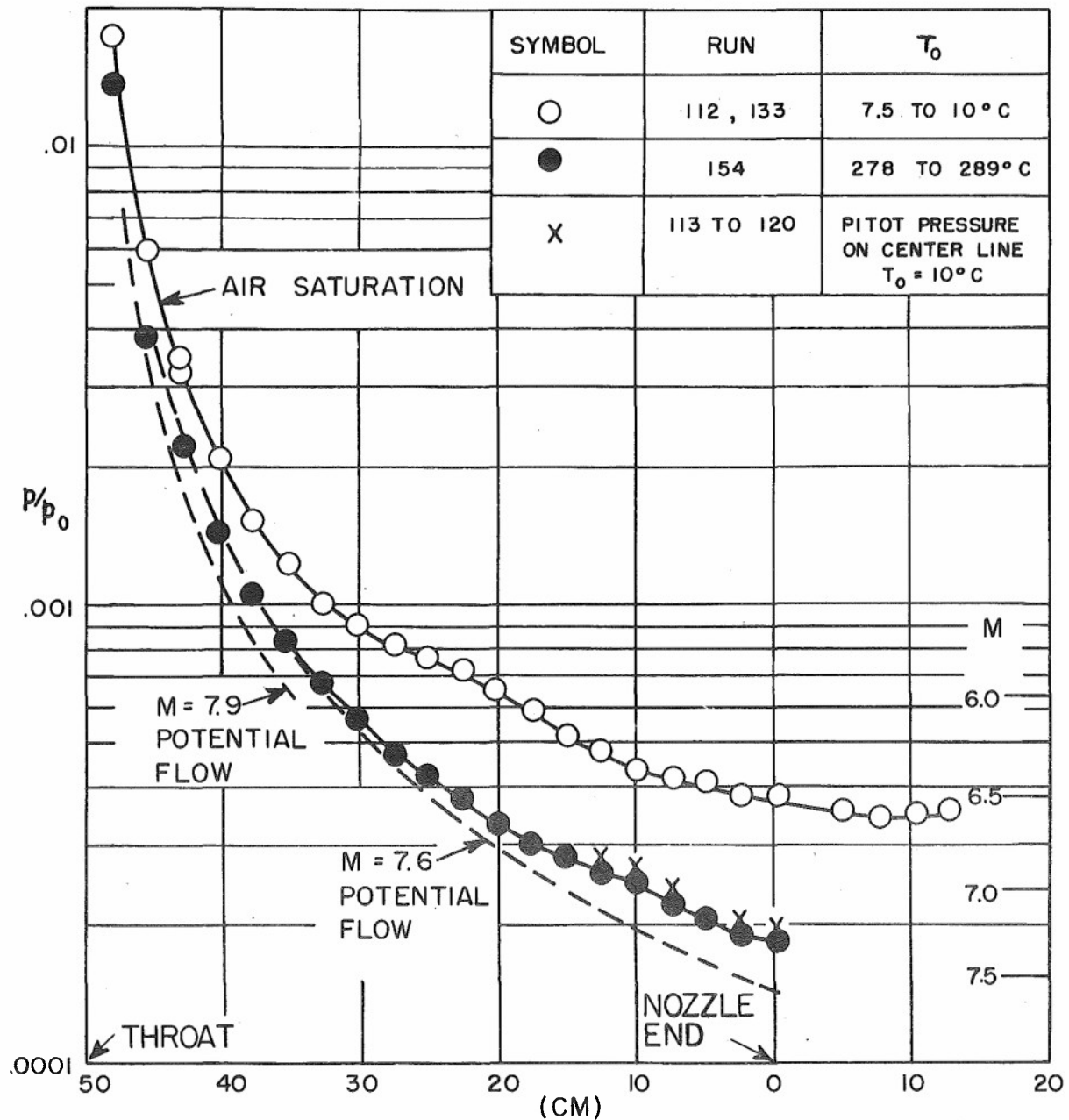


FIG. 12

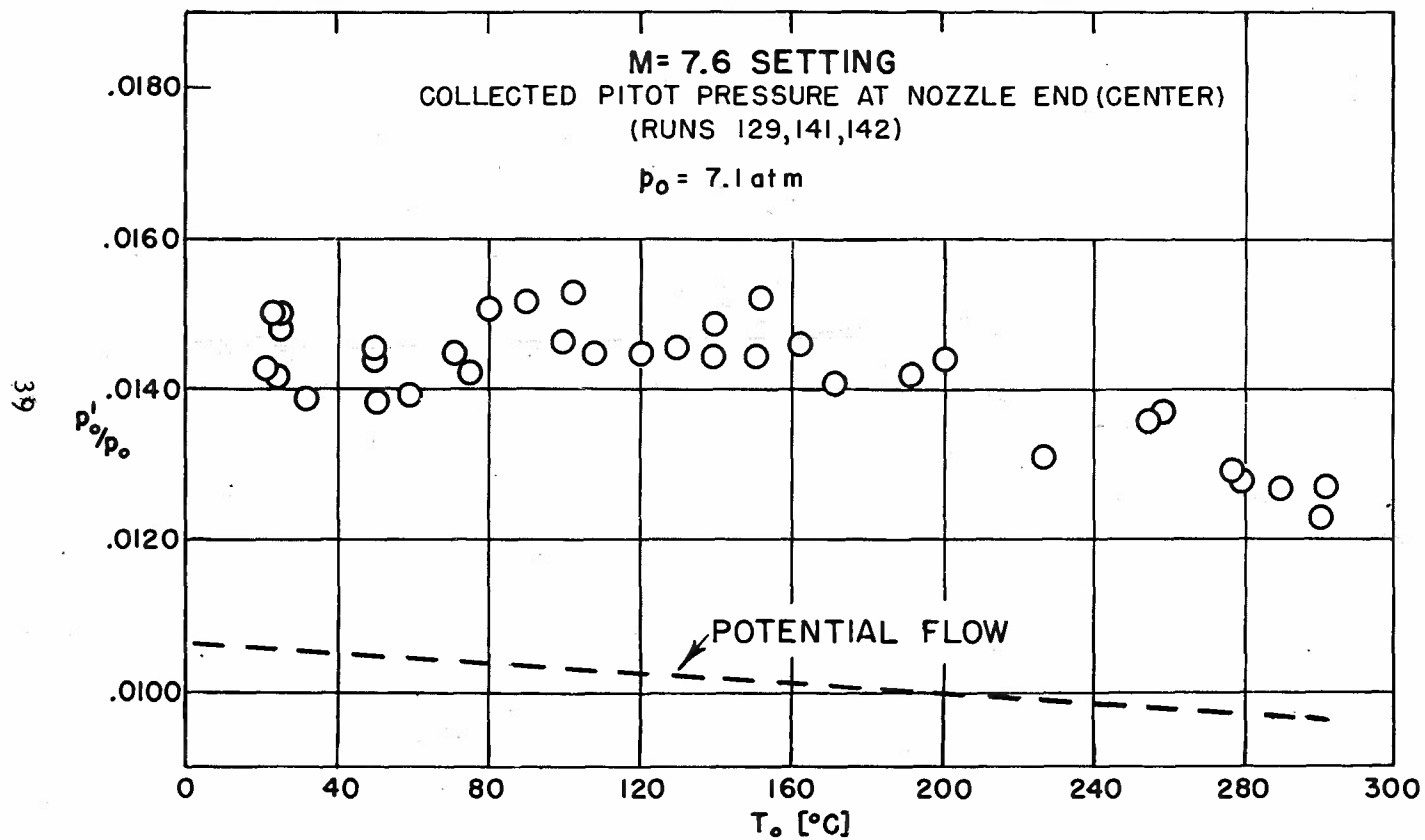
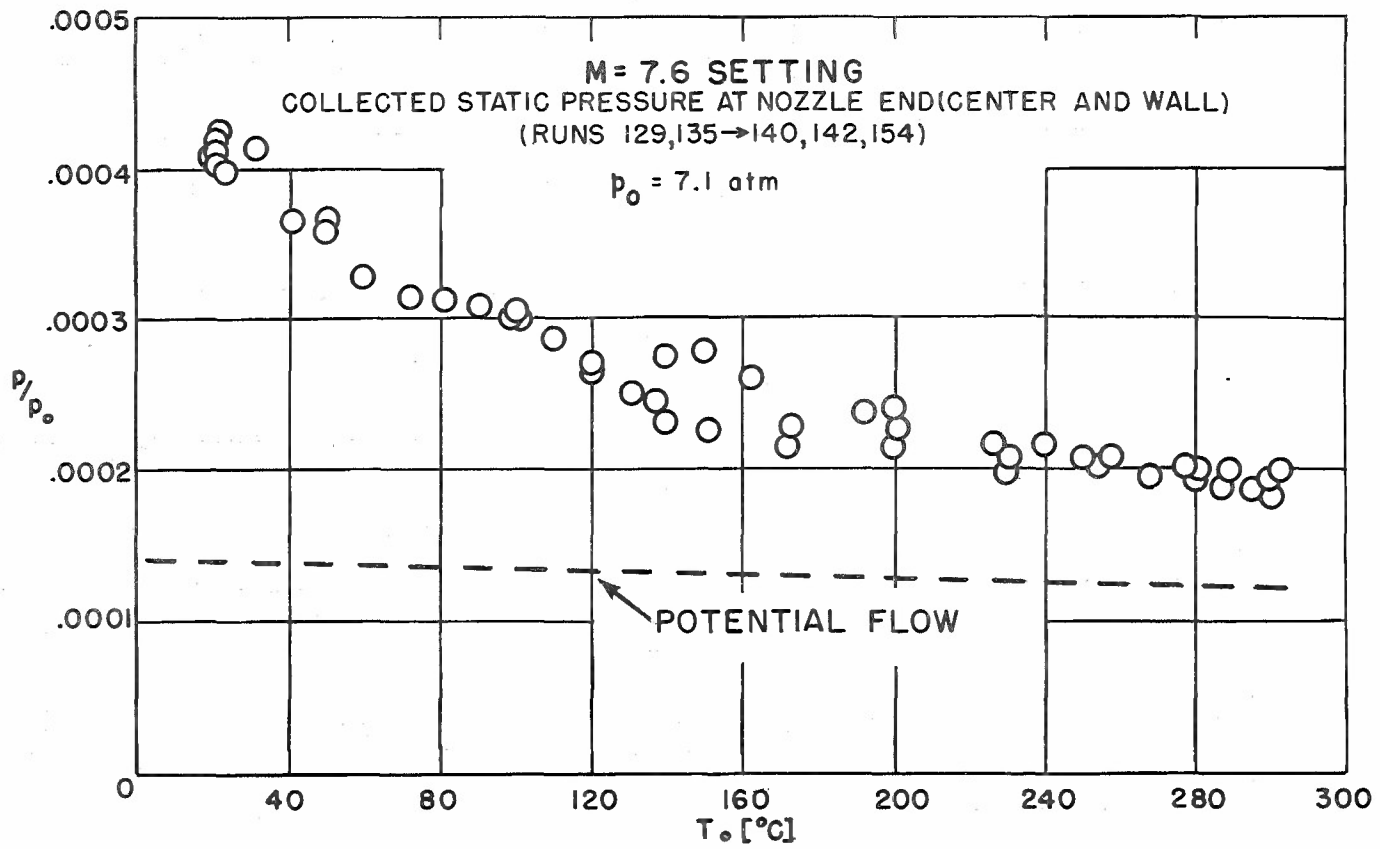
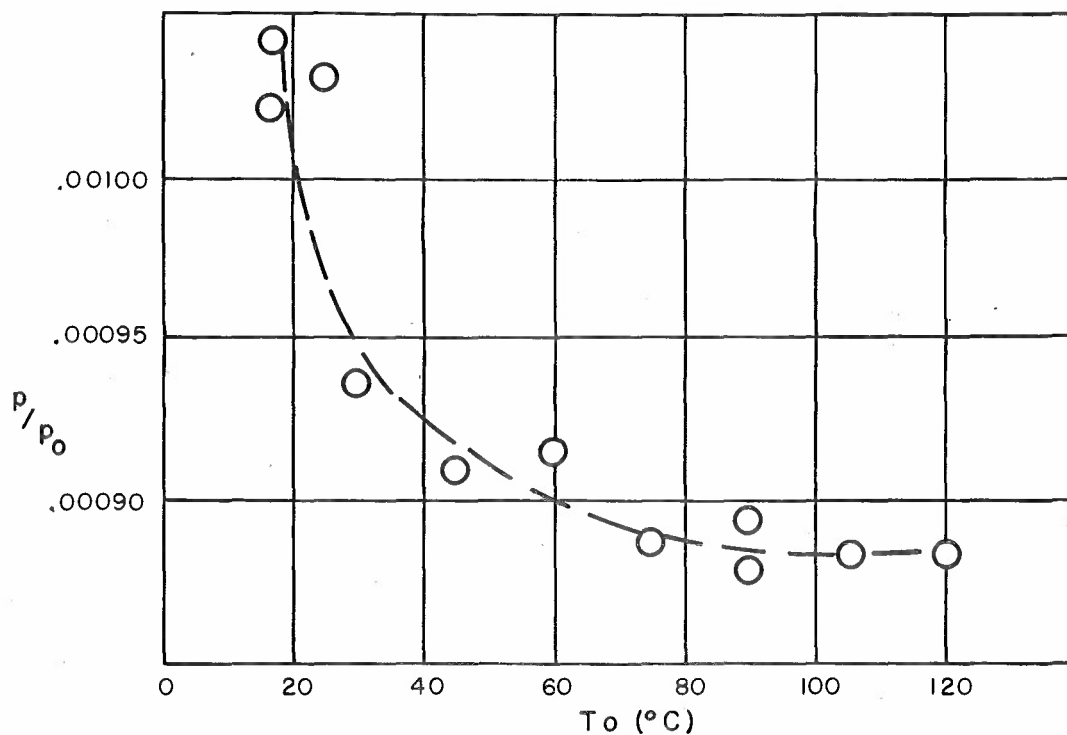
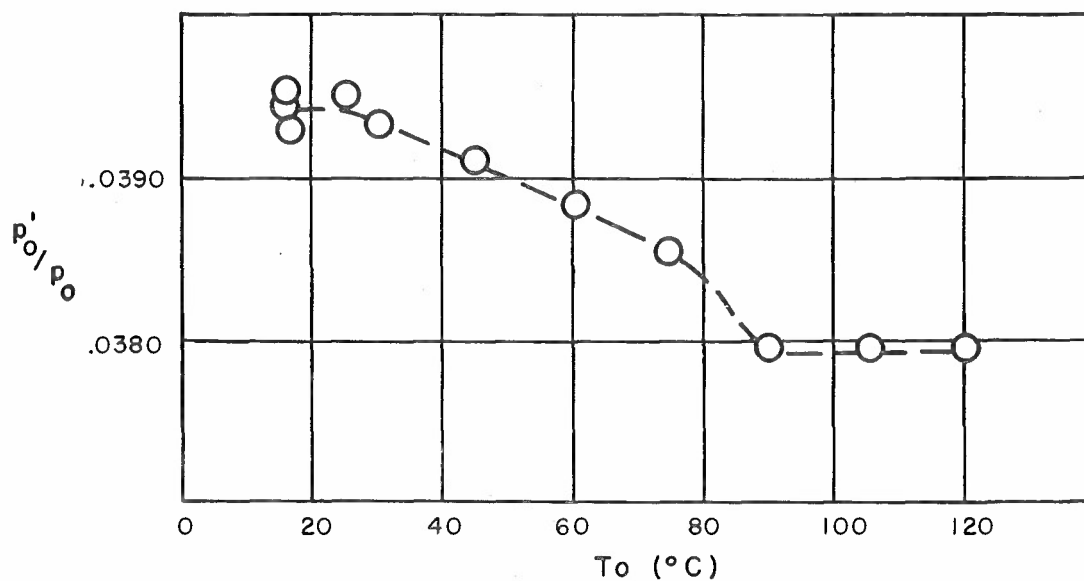


FIG. 13



M = 6 SETTINGp₀ = 3.04 ATM

WALL STATIC PRESSURE AT NOZZLE END
RUNS 159, 161



PITOT PRESSURE ON CENTER OF NOZZLE END
RUNS 158, 159, 161

M = 6 SETTING
COLLECTED M FROM PITOT AND
STATIC PRESSURE AT NOZZLE END

$P_o = 3.04 \text{ ATM}$
RUNS 158, 159, 161

X M FROM $P_{o'}/P_o$
O M FROM P/P_o

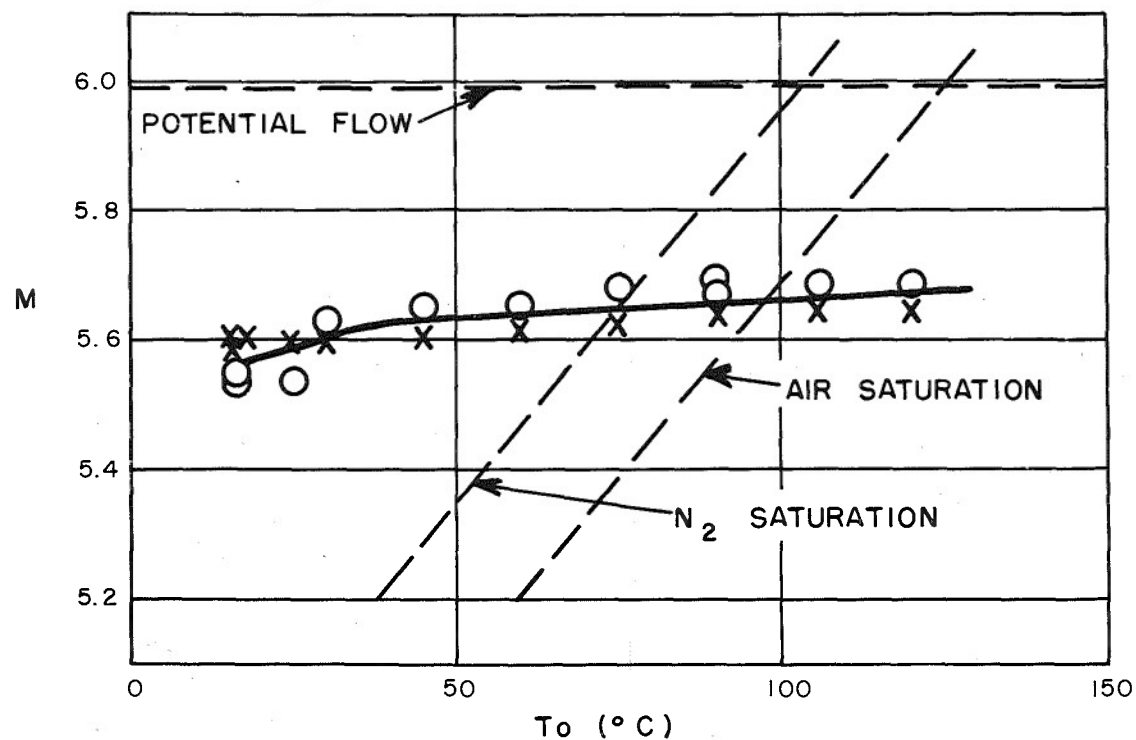
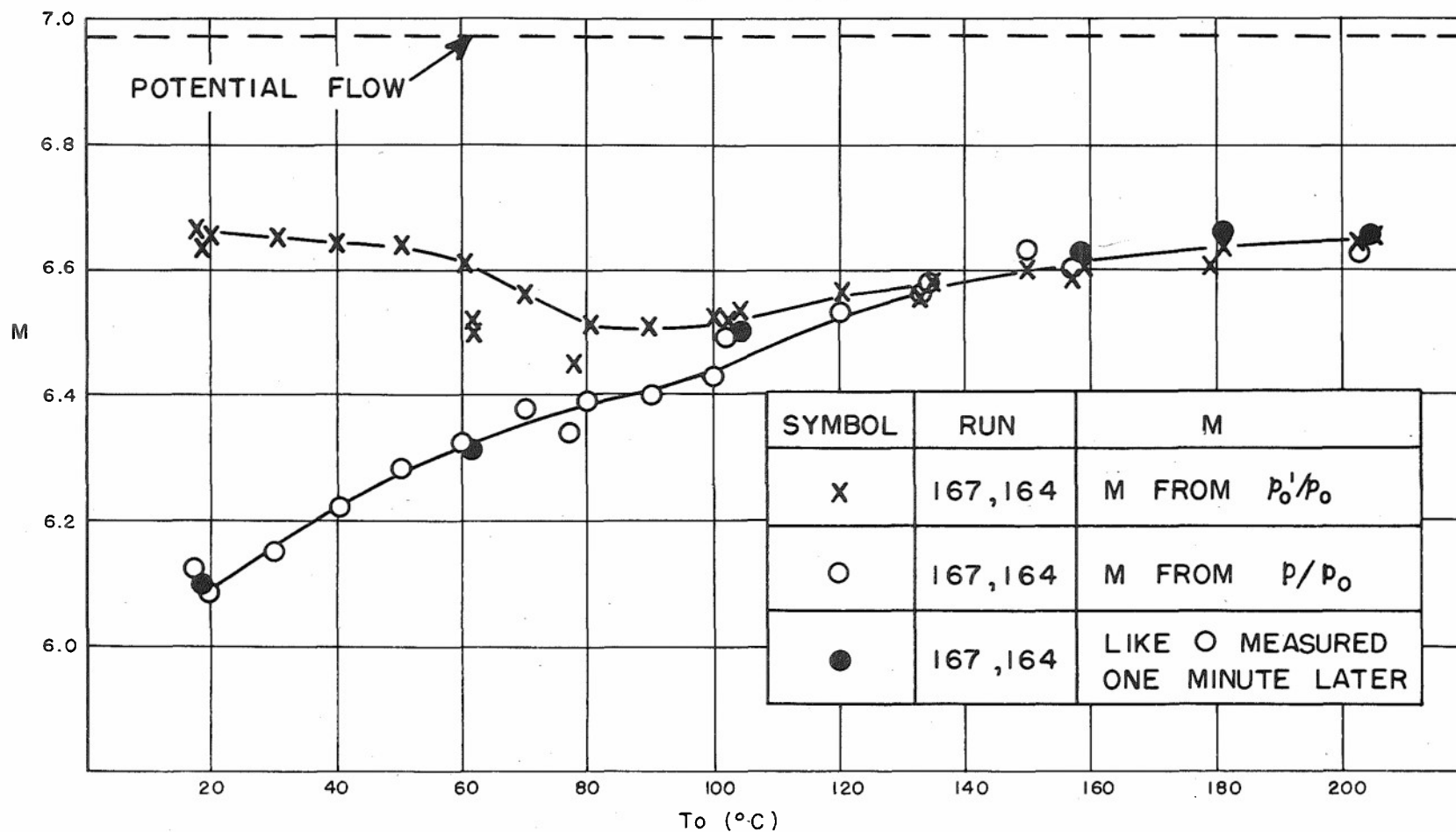


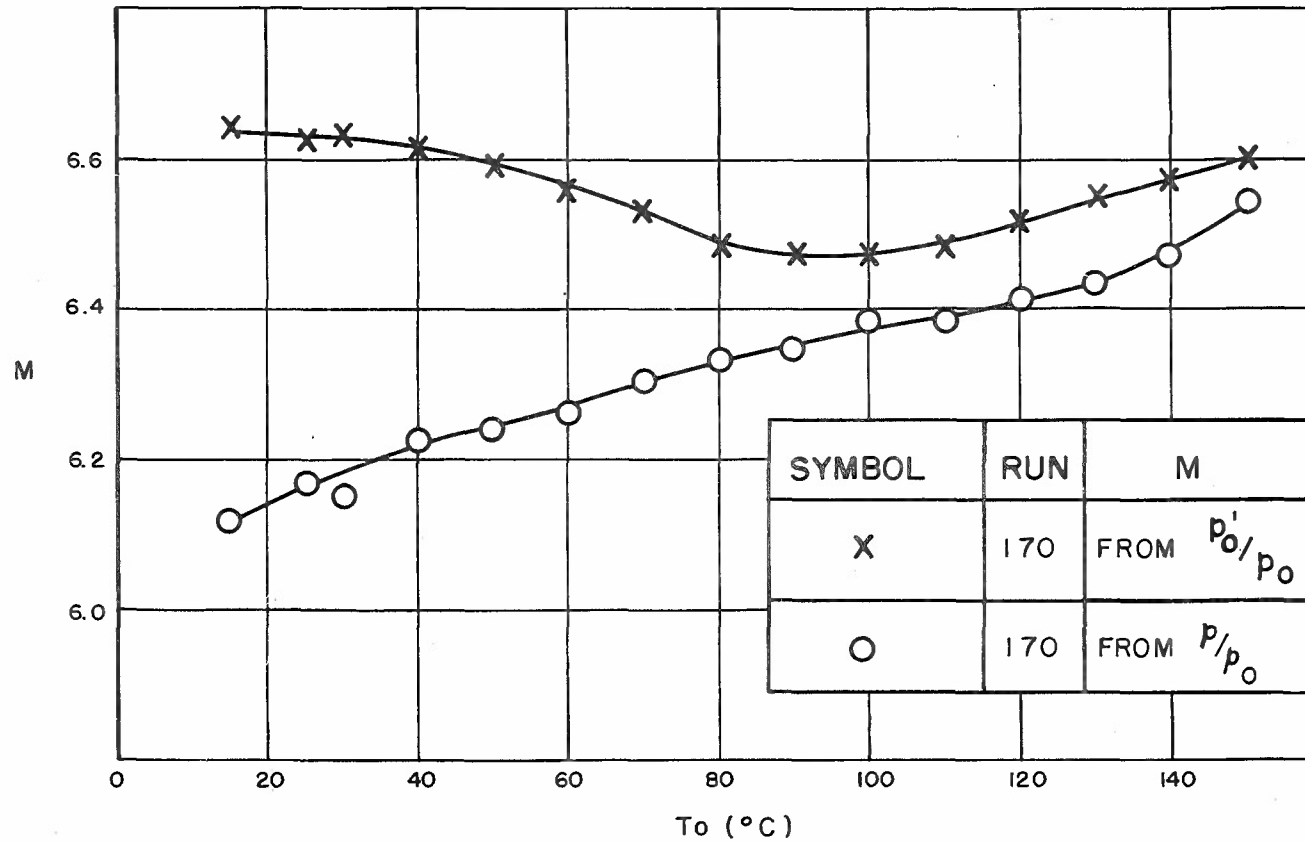
FIG.15

M = 7 SETTING
COLLECTED M FROM PITOT AND STATIC PRESSURE AT NOZZLE END
 $p_0 = 5.07 \text{ ATM} = \text{CONST.}$



M = 7 SETTING

COLLECTED M FROM PITOT AND STATIC PRESSURE AT NOZZLE END
 p_o VARIED TO KEEP $Re/l \sim 7 \times 10^4 / \text{CM} \sim \text{CONST.}$



M = 7 SETTING

COLLECTED M FROM PITOT AND STATIC PRESSURE AT NOZZLE END
 P_0 VARIED TO KEEP $P_0/P_{atm} = 4.85 = \text{CONST.}$

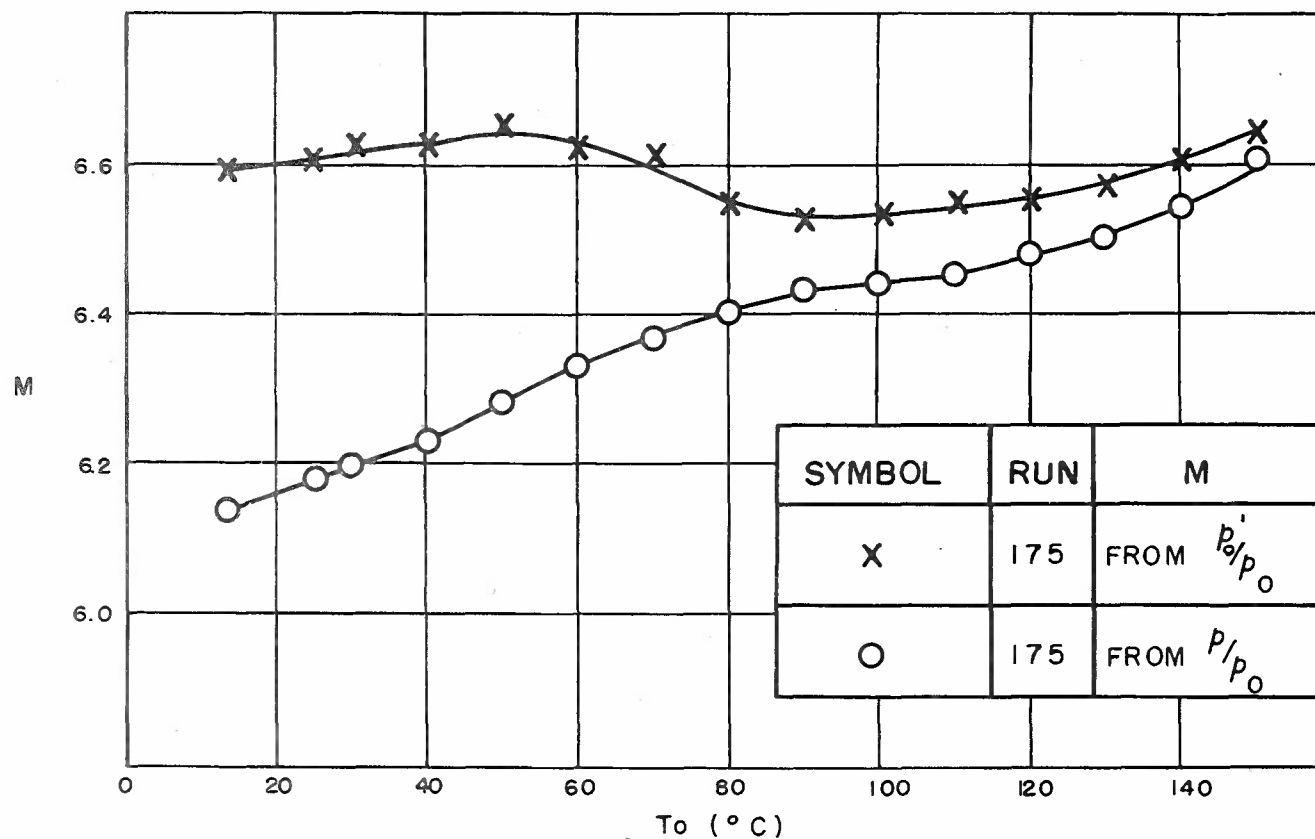
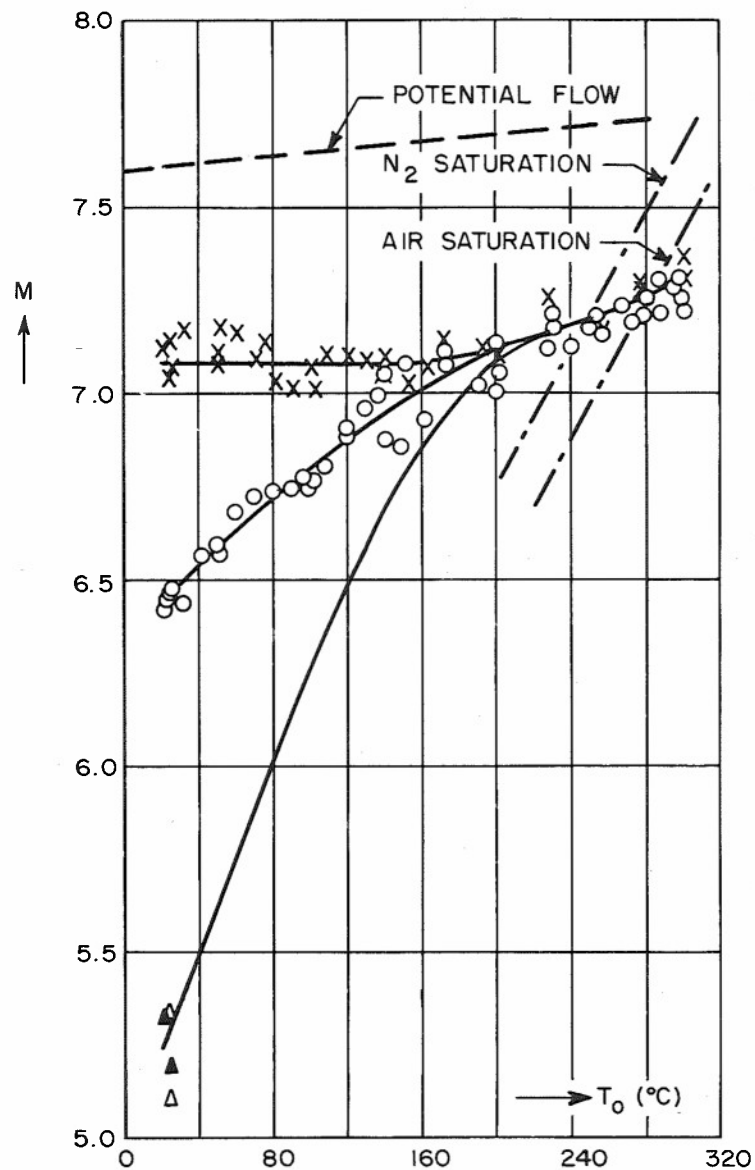


FIG. 18



$M=7.6$ SETTING
COLLECTED M FROM VARIOUS
METHODS AT NOZZLE END
 $P_0 = 7.1$ ATM

SYMBOL	M FROM
X	PITOT PRESSURE
O	STATIC PRESSURE
—	RAYLEIGH FORMULA
Δ	CONE PRESSURE 40° CONE
▲	CONE PRESSURE 80° CONE

FIG. 19

M = 9 SETTING $p_0 = 7.8$ ATM
 COLLECTED M FROM PITOT AND STATIC PRESSURE AT NOZZLE END

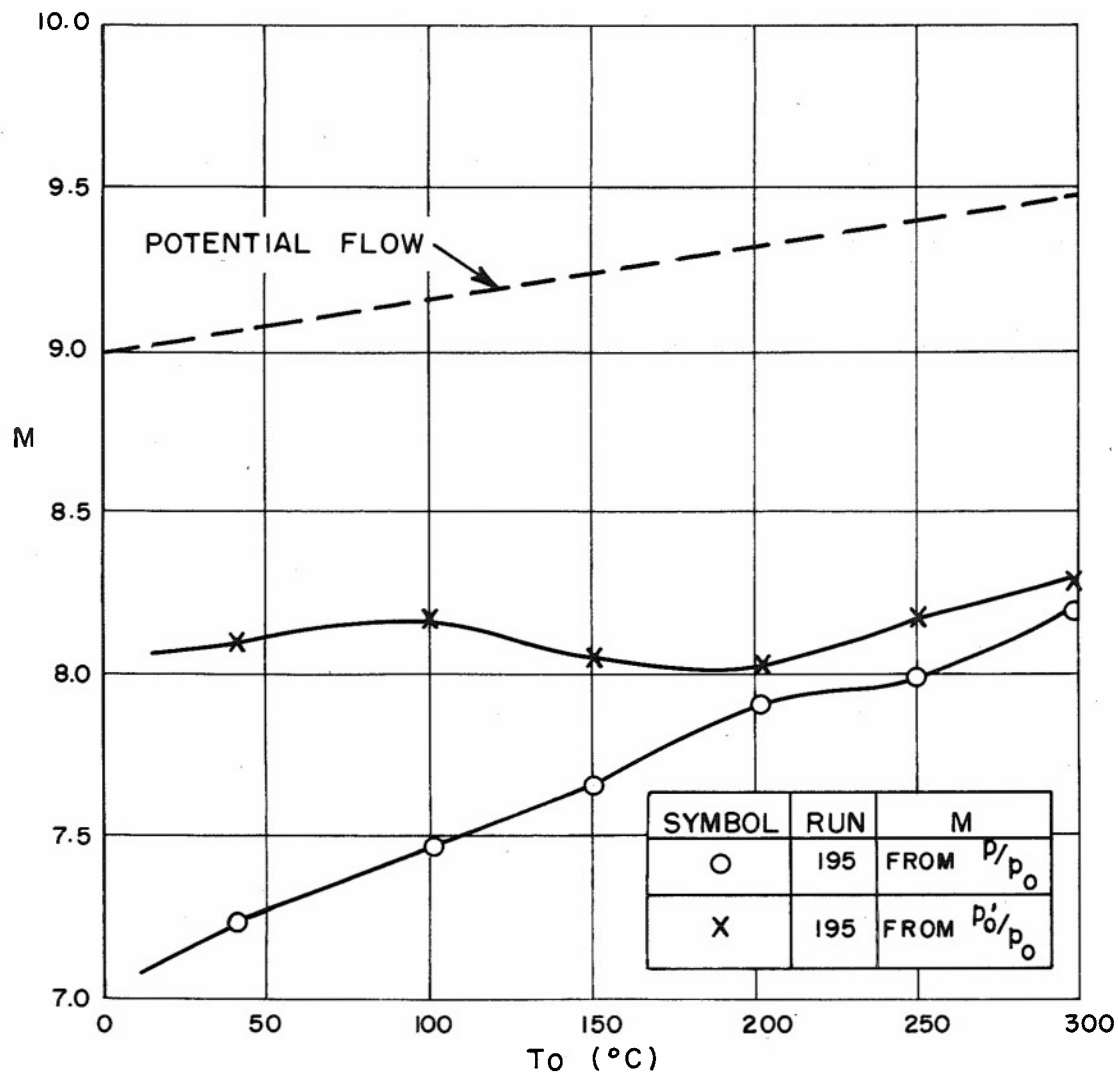
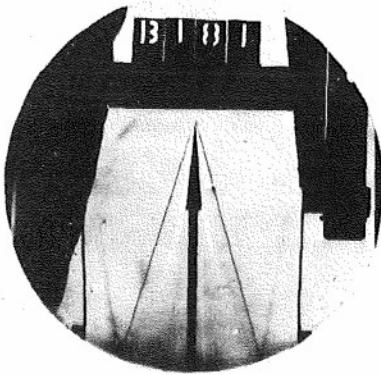


FIG.20

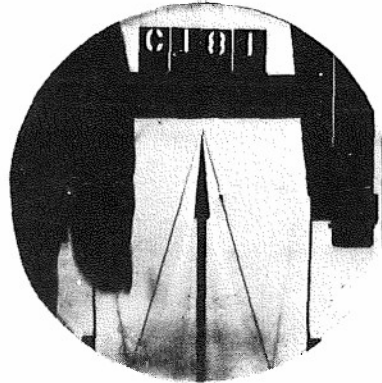
M = 7.6 SETTING

FIG. 21

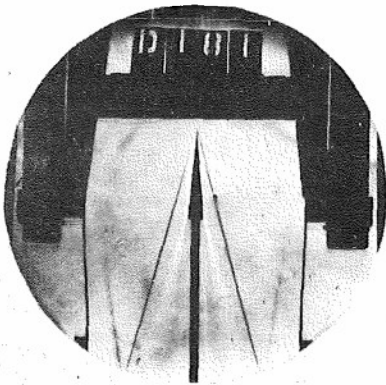
10° WEDGE, $\rho_0/\rho_{\text{atm}} = 4.83 = \text{CONSTANT}$



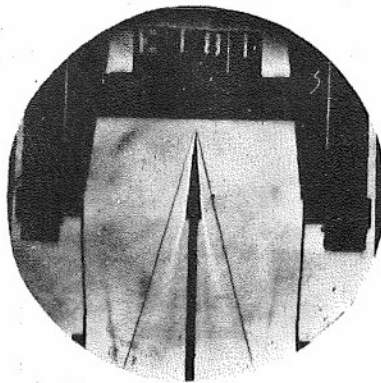
To = 41° C



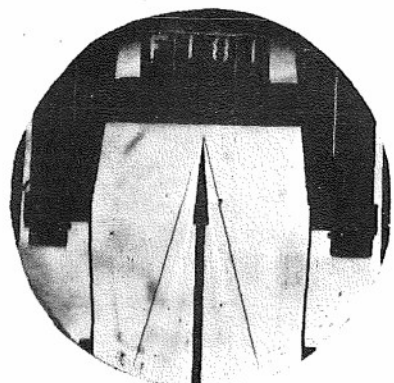
To = 71° C



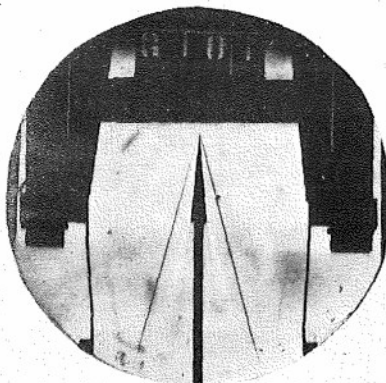
To = 101° C



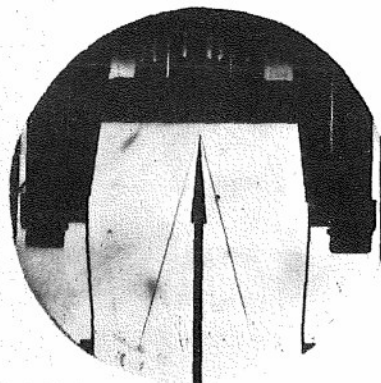
To = 119° C



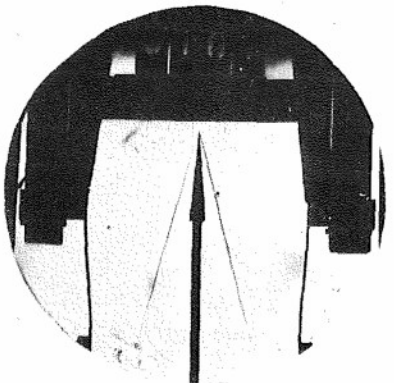
To = 140° C



To = 152° C



To = 171° C



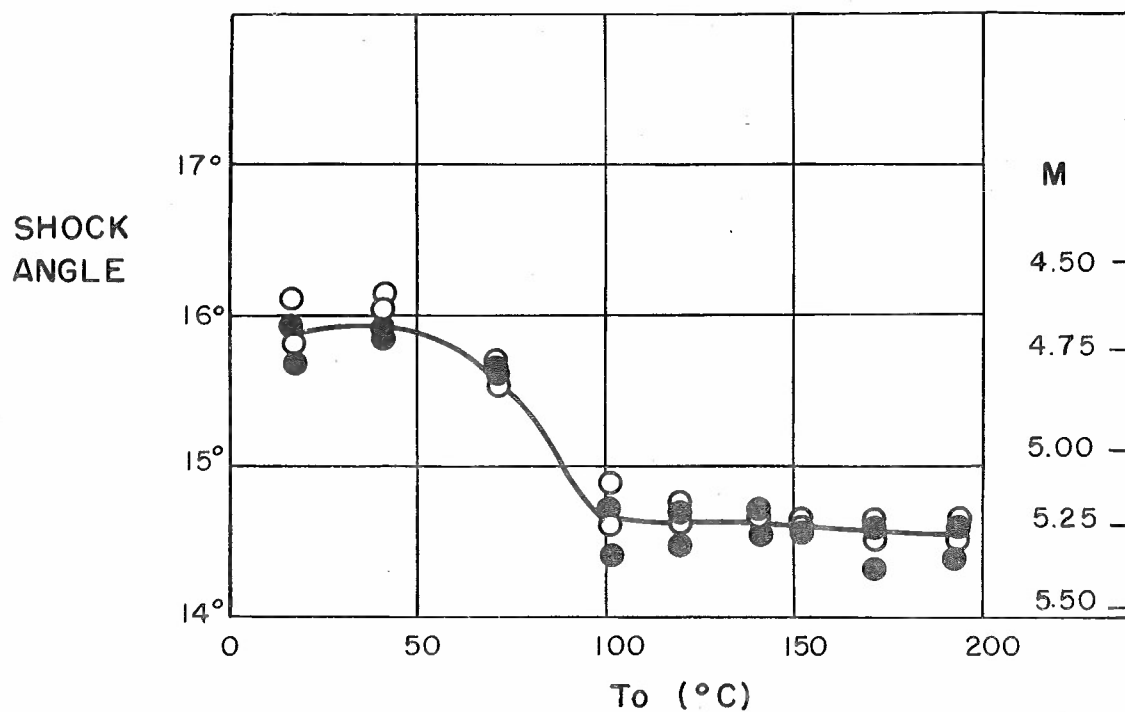
To = 193° C

FIG. 22

M = 7 SETTING
SHOCK ANGLE ON 10° WEDGE

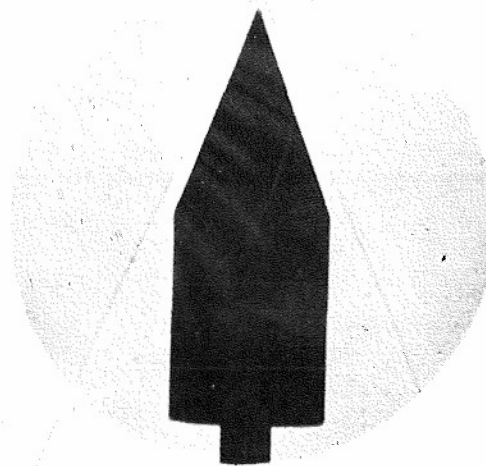
$$\rho_o / \rho_{atm} \quad 4.83 = \text{CONSTANT}$$

○ WEDGE SIDE 1 } TWO OBSERVERS
● WEDGE SIDE 2 }

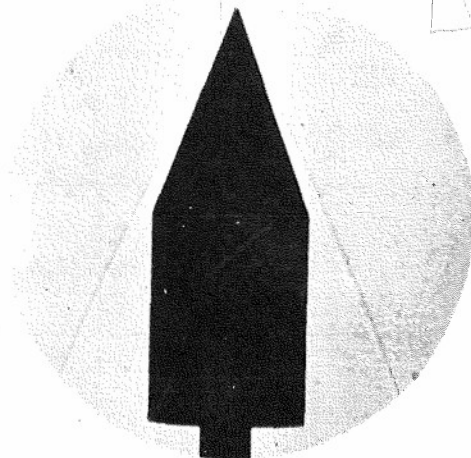


M=7.6 SETTING
40° CONE, $P_0 = 7.1 \text{ ATM}$

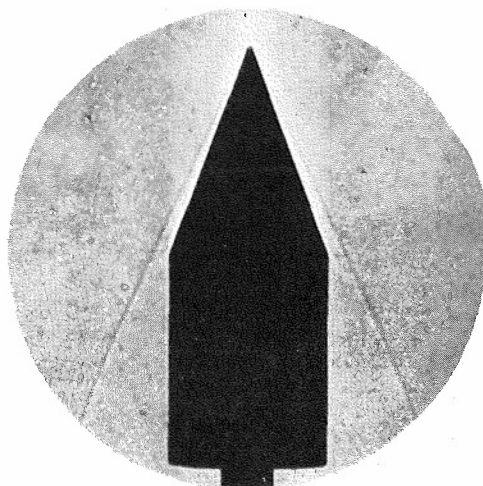
FIG. 23



$T_0 = 25^\circ\text{C}$



$T_0 = 142^\circ\text{C}$

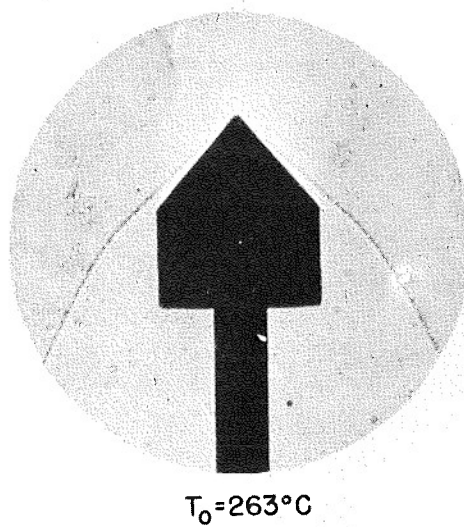
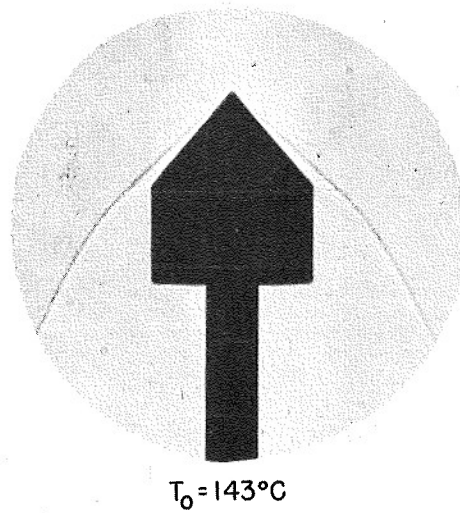
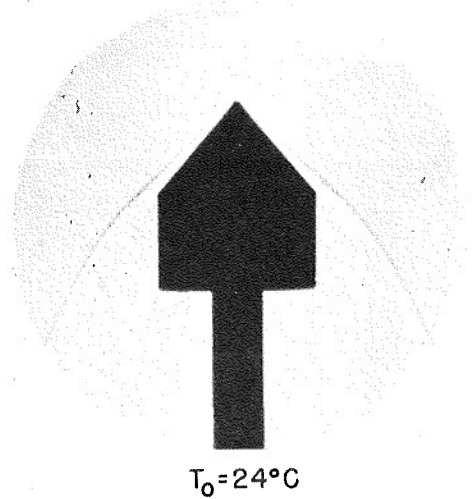


$T_0 = 265^\circ\text{C}$
50

$\mu = 7.5$
 $B_w = 24^\circ$
 $25\frac{1}{4}$

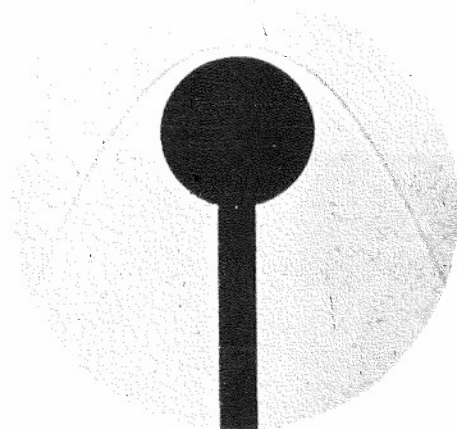
NAVORD REPORT 1742
M=7.6 SETTING
80° CONE, $P_0 = 7.1$ ATM

FIG. 24

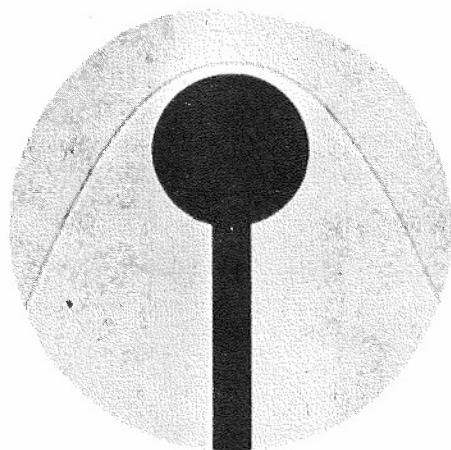


NAVORD REPORT 1742
M=7.6 SETTING
SPHERE-2 CM DIAM, $P_0 = 7.1$ ATM

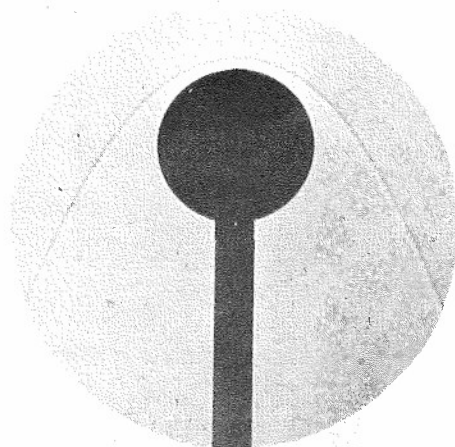
FIG. 25



$T_0 = 80^\circ\text{C}$



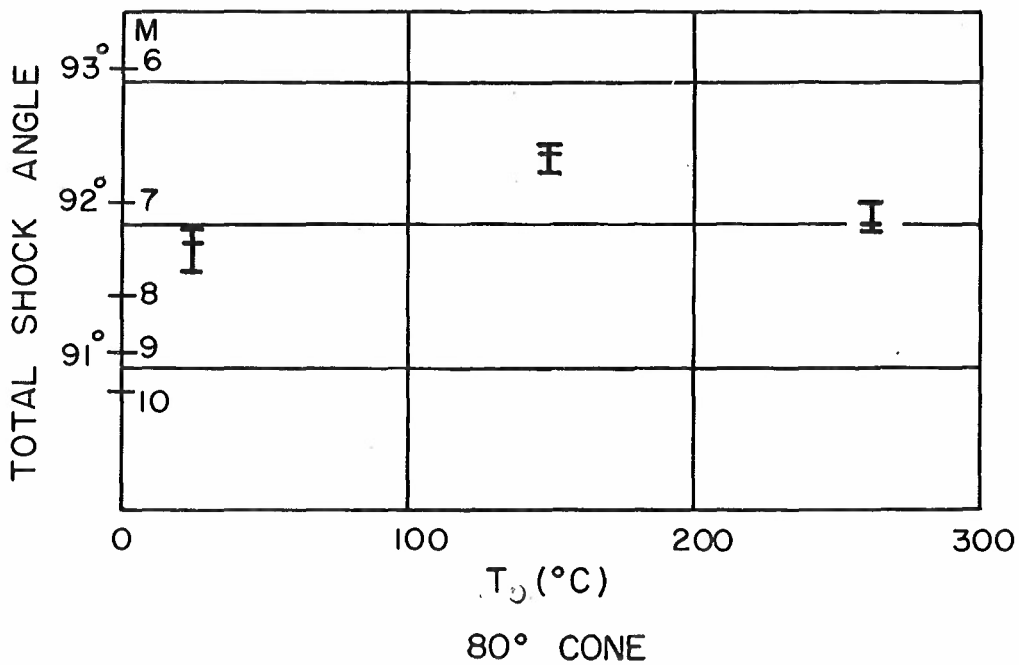
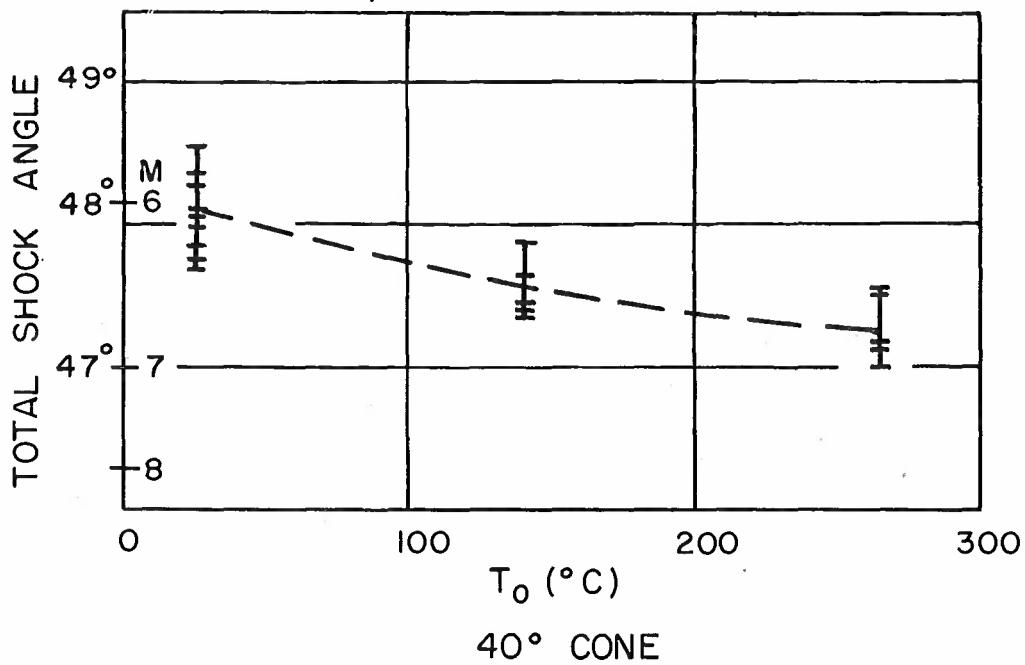
$T_0 = 145^\circ\text{C}$



$T_0 = 276^\circ\text{C}$

M = 7.6 SETTING
SHOCK ANGLE ON CONES
 $p_0 = 7.1$ ATM

FIG.26

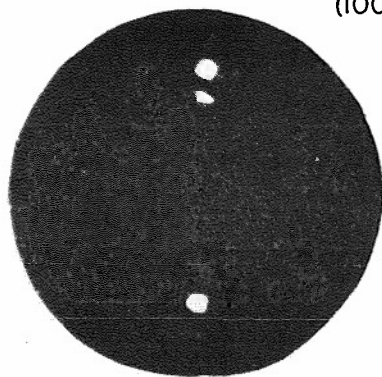


M = 7.6 SETTING

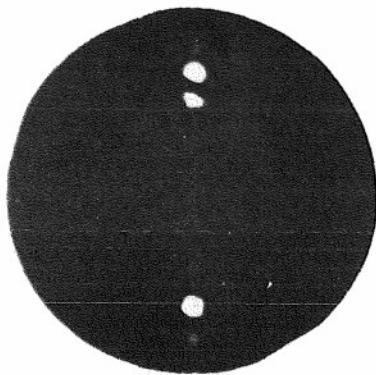
$p_0 = 7.1$ ATM

FIG. 27

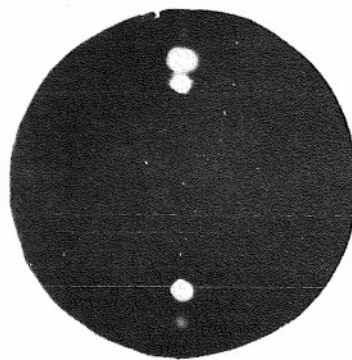
LIGHT SCATTERING DATA
(100 WATT WESTERN UNION ARC)



NO BLOW

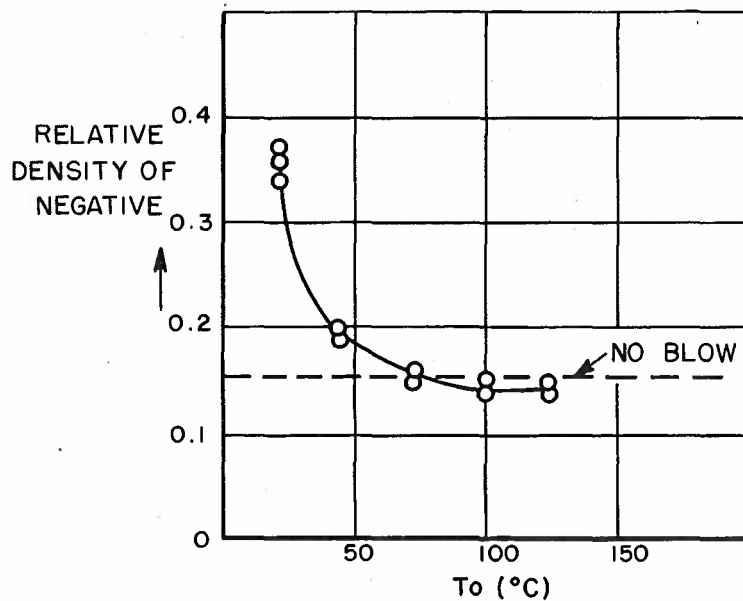


$T_o = 22^\circ\text{C}$



$T_o = 42^\circ\text{C}$

INTENSITY OF SCATTERED LIGHT
(WESTON PHOTO DENSITOMETER)



M = 7 SETTING

FIG.28

PITOT PRESSURE ACROSS CENTER
OF NOZZLE EXIT AREA

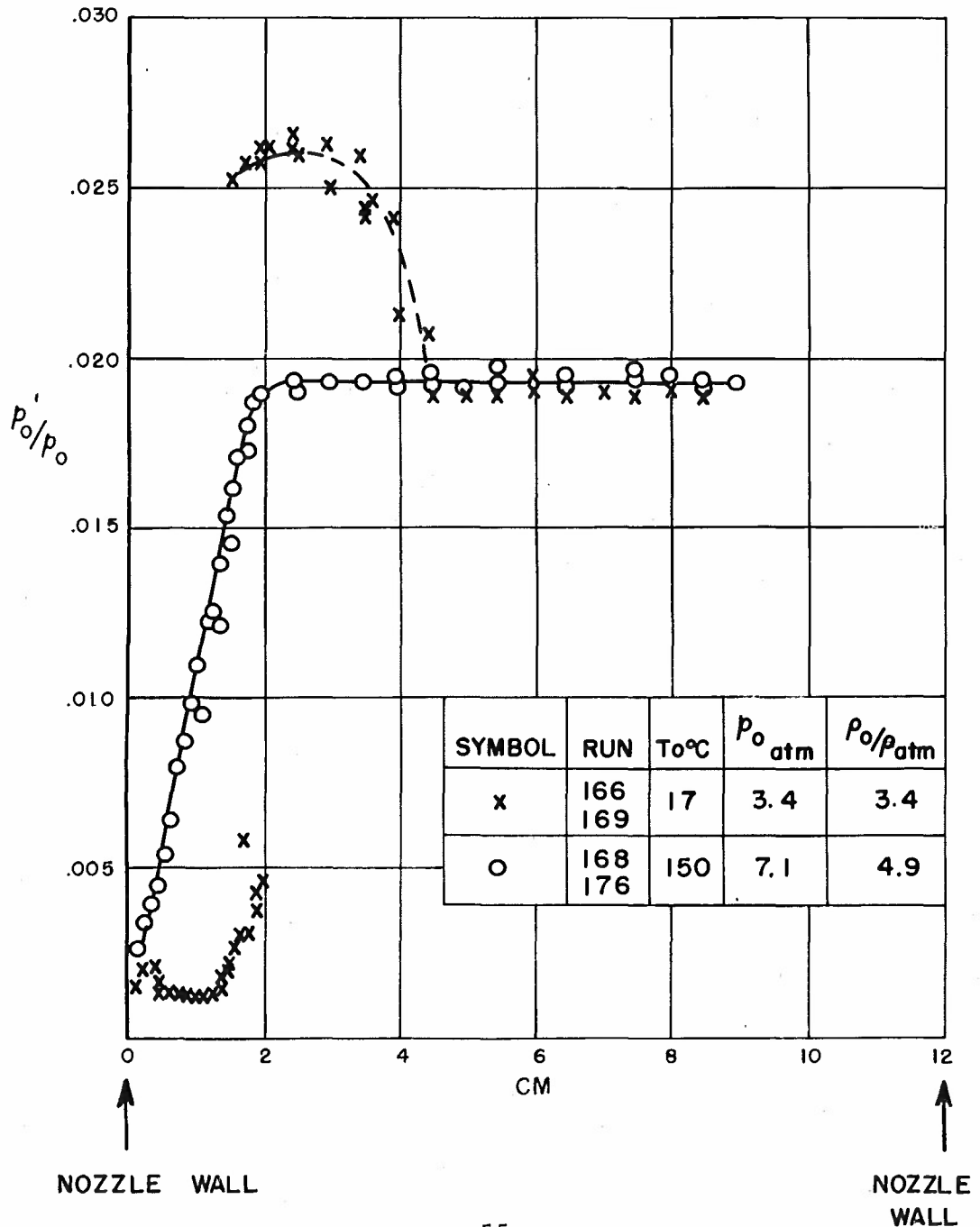
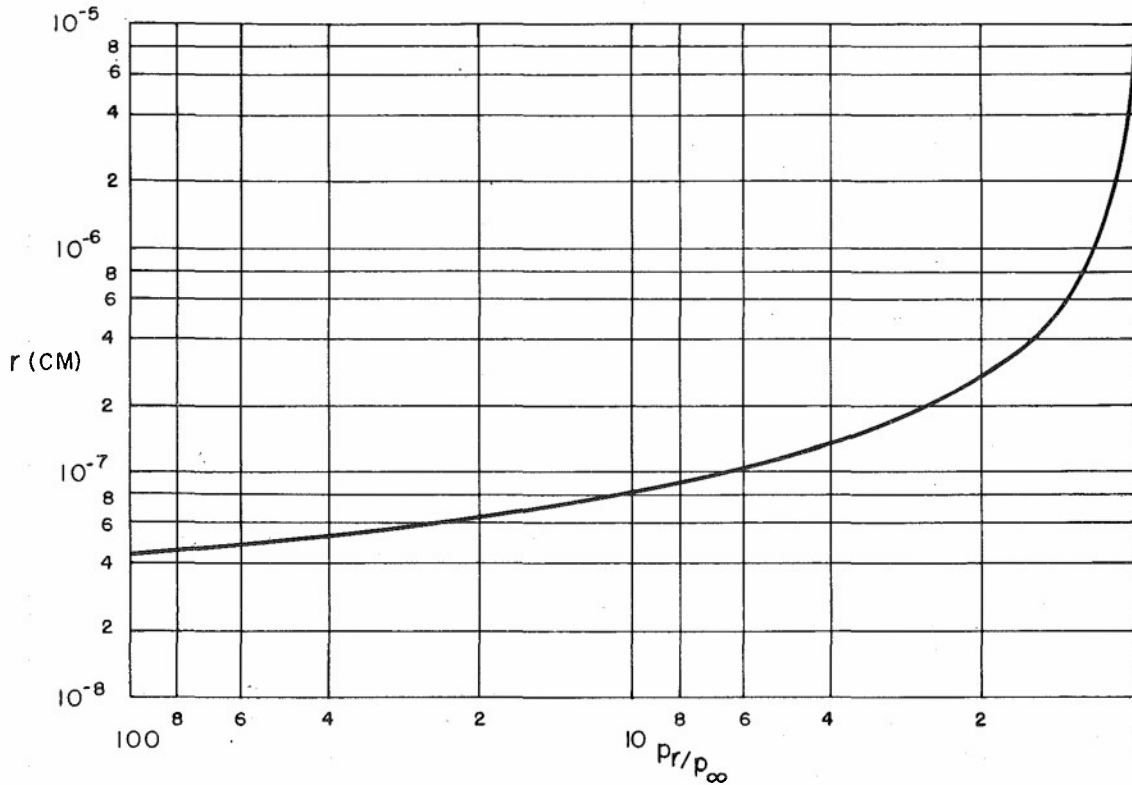


FIG. 29

ESTIMATE OF CRITICAL DROPLET RADIUS AS A FUNCTION OF SATURATION RATIO FOR AIR



ESTIMATE OF NUMBER OF WATER VAPOR NUCLEI PRESENT AT POINT OF AIR SATURATION AS A FUNCTION OF RADIUS FOR NOZZLE SETTING $M = 7.6$, $P_0 = 7$, $T_0 = 15^\circ\text{C}$

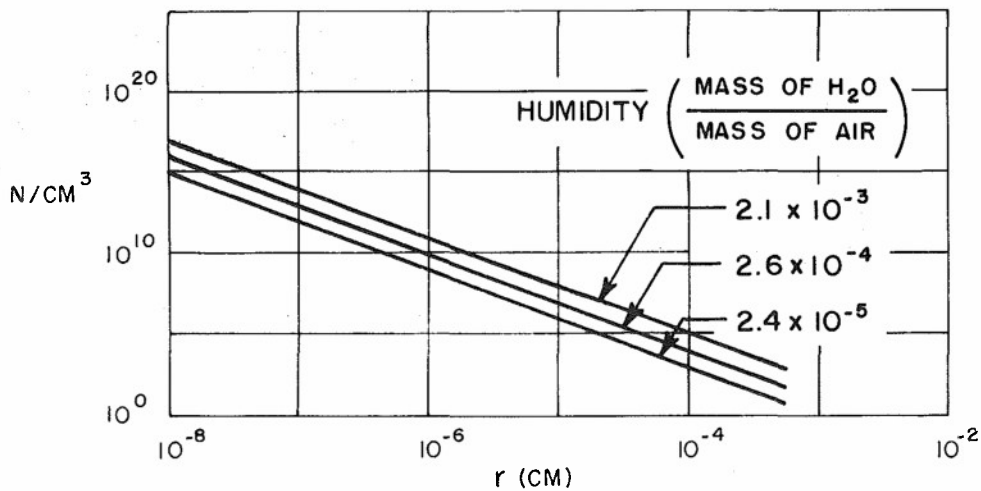
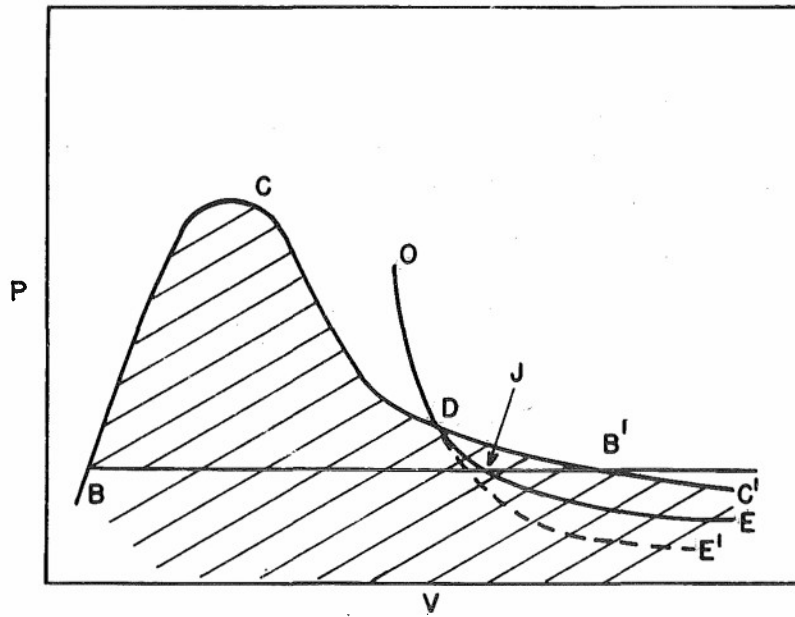


FIG. 30 & 31

PRESSURE VS VOLUME



SOUND SPEED $= \sqrt{dp/d\rho}$ VS VOLUME

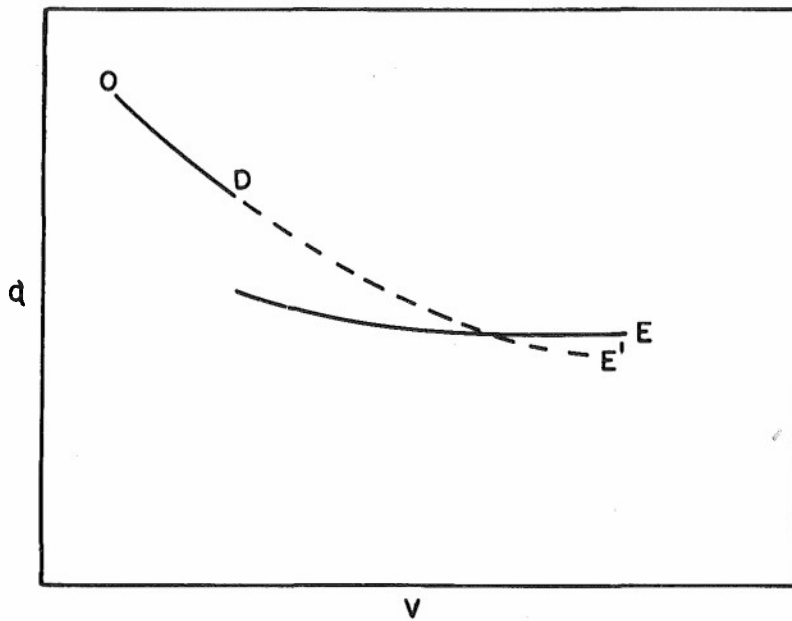
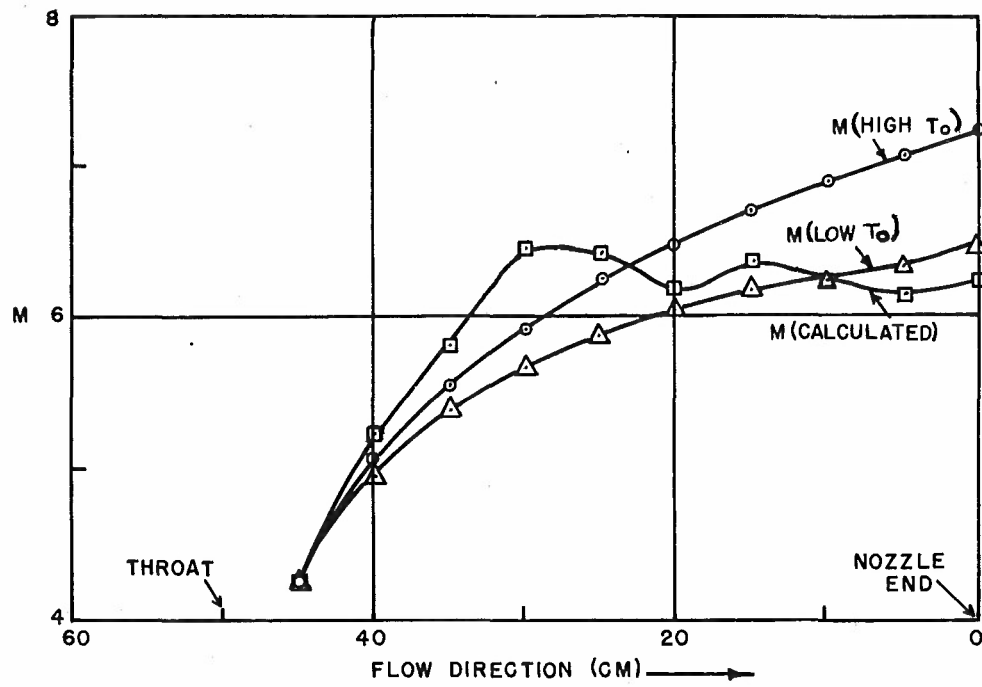


FIG. 32

 $M=7.6$ SETTING $p_o=7.1$ ATM

M = 7.6 SETTING

$p_0 = 7.1$ ATM

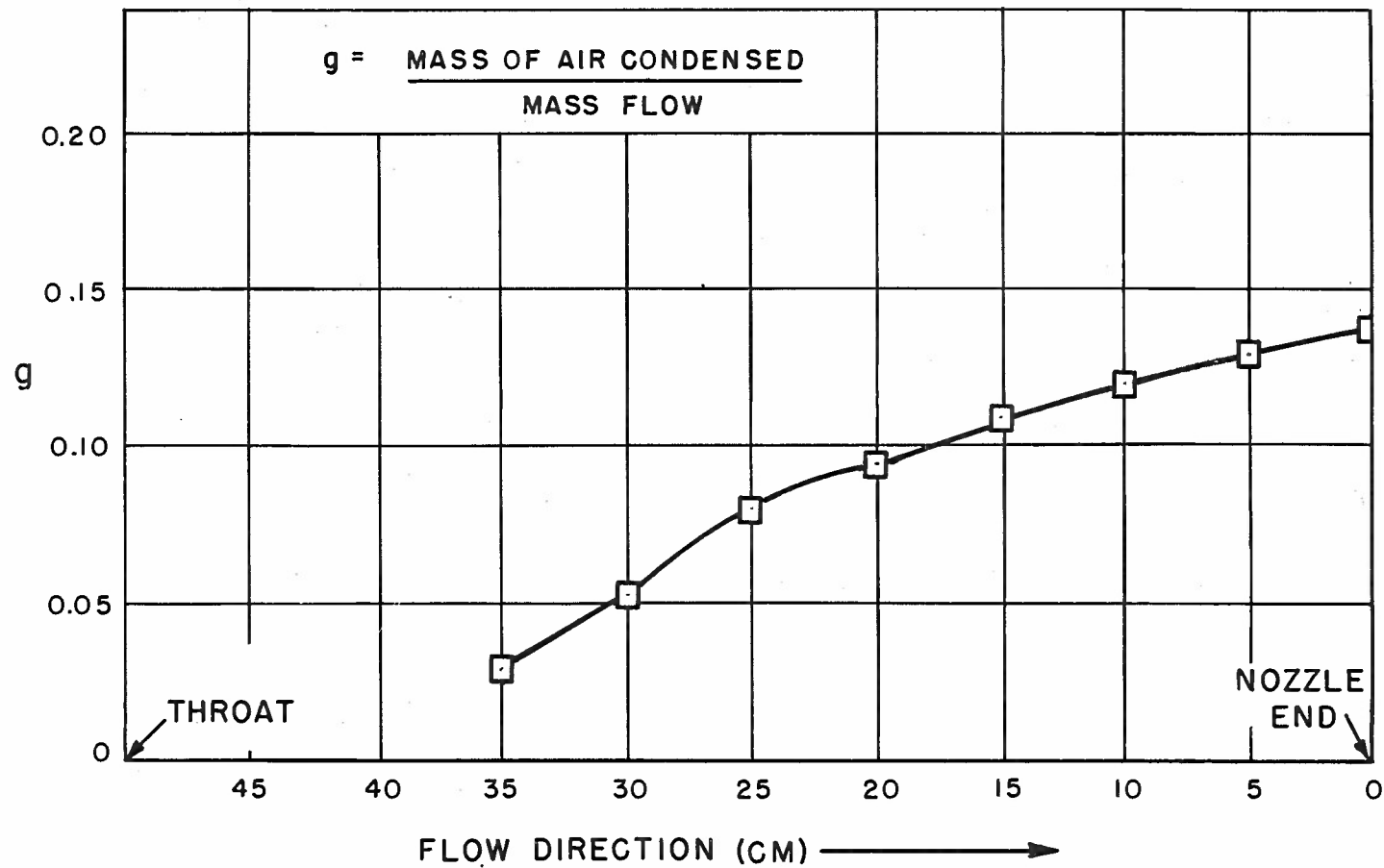
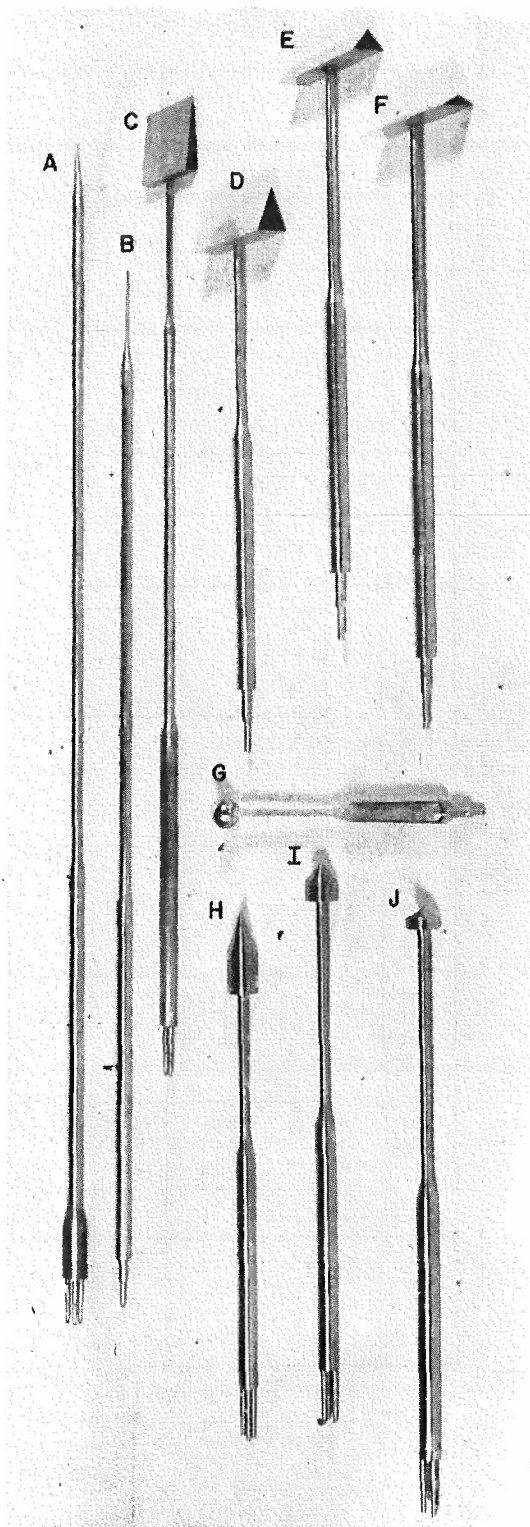


FIG.33

PROBES AND MODELS

FIG. 34

- A - 10° CONE, CENTER LINE
STATIC PROBE
B - CENTER LINE PITOT
PROBE
C - 10° WEDGE
D - 40° WEDGE
E - 80° WEDGE
F - 120° WEDGE
G - SPHERE
H - 40° CONE
I - 80° CONE
J - 120° CONE



"A" EXTERNAL DISTRIBUTION FOR BASIC AERODYNAMICS (X2)

15 Sept. 50

No. of
Copies

1	Chief, Bureau of Ordnance, Navy Department	
1	Capt. C. H. Lyman, Rea	
1	Re3	
1	Re9	
1		
1	Commander, Naval Ordnance Test Station, Inyokern, China Lake,	
	California	
1	Dr. A. Bennett	
1	Reports Unit (Library)	
1	Commanding Officer, Naval Proving Ground, Dahlgren, Virginia	
1	Dr. C. C. Bramble	
1	Commanding Officer, U. S. Naval Air Missile Test Center,	
	Point Mugu, California	
1	Director, Applied Physics Laboratory Development Contract Officer	
	Johns Hopkins University	Applied Physics Lab.
	8621 Georgia Avenue	VIA The Johns Hopkins Univ.
	Silver Spring, Maryland	8621 Georgia Avenue
		Silver Spring, Maryland
1	Prof. J. D. Akerman	Inspector of Naval Material
	Dept. of Aero. Engineering	VIA Federal Building
	University of Minnesota	Milwaukee 2, Wisconsin
	Minneapolis, Minnesota	
2	Chief Scientist, Office of Air Research, Air Materiel Command,	
	Wright-Patterson Air Force Base, Dayton, Ohio	
1	Armour Research Foundation, 25 West 33rd Street, Chicago 16,	
	Illinois, Dr. Le Van Griffis	
1	Director	Development Contract Officer
	New Mexico School of Mines	VIA New Mexico School of Mine
	Research and Development Division	Socorro, New Mexico
	Socorro, New Mexico	
1	Chairman, Guided Missile Committee	Development Contract Officer
	Project METEOR	Massachusetts Institute of
	Mass. Institute of Technology	VIA Technology
	Cambridge 38, Massachusetts	Cambridge 38, Massachusetts
1	Guided Missiles Library, Room 22-001	
1	Commanding General, Air University, Maxwell Air Force Base,	
	Alabama	

BASIC AERODYNAMICS (X2) (Cont.)

- 1 Rand Corporation, 1500 4th Street, Santa Monica, California
Dr. R. W. Kruger,
- 1 Director, Project SQUID, Princeton University, Princeton, N. J.
VIA Inspector of Naval Material, 17 Brief Ave., Upper Darby,
Pa., Philadelphia, Pa.
- 3 Chief, Bureau of Aeronautics, Navy Department
 - 1 Capt. W. S. Diehl
 - 1 Dr. O. E. Lancaster
 - 1 TD-4
- 1 Chief, Bureau of Ships, Navy Department
- 1 Director, David Taylor Model Basin
 - 1 Aeromechanics Division
- 5 Office of Naval Research, Navy Department
 - 1 Mathematics Branch
 - 1 Chief, Fluid Mechanics Branch
- 1 Director, Naval Research Laboratory, Anacostia Station
 - 1 Mr. G. Irwin, Superintendent, Mechanics Division
- 1 Commanding Officer, U. S. Naval Administrative Unit, The
Artillery School, Antiaircraft and Guided Missile Branch,
Fort Bliss, Texas
- 1 Superintendent, U. S. Naval Postgraduate School, Naval Academy,
Annapolis, Md.
- 1 Commanding General, Air Force, National Defense Building
 - 1 Scientific Advisory Board
 - 1 AC/AS-4, DRE-3
- 1 Commanding General, Air Materiel Command, Wright Field, Dayton,
Ohio
 - 1 Mr. D. Shore
 - 1 TSEON-2
 - 1 MCIDXD
- 1 Commanding General, Aberdeen Proving Ground, Aberdeen, Md.
 - 1 Director, Ballistic Research Laboratories
 - 1 Dr. A. C. Charters
 - 1 Mr. C. L. Poor
- 1 Office of the Chief of Ordnance, National Defense Building
 - 1 ORDTX-AR

BASIC AERODYNAMICS (X2) (Cont.)

2	Chairman, The Research and Development Board, National Defense Bldg., Information Requirement Board, Room 3D1075	
1	Director, National Bureau of Standards, Connecticut Avenue at Upton St., Washington 25, D. C.	
1	Dr. G. Schubauer	
1	Director, National Advisory Committee for Aeronautics, 1724 F St., N. W., Washington, D. C.	
1	Dr. J. W. Crowley	
1	Dr. I. H. Abbott	
1	Office of Aeronautical Intelligence	
1	Director, Ames Aeronautical Laboratory, Moffett Field, Calif.	
1	Mr. W. G. Vincenti	
1	Mr. H. J. Allen	
1	Director, Lewis Flight Propulsion Lab., Cleveland, Ohio	
1	Mr. John C. Evvard	
1	Mr. Abe Silverstein	
1	Director, Langley Aeronautical Laboratory, Langley Field, Va.	
1	Mr. John Stack	
1	Mr. Carl Kaplan	
1	University of Michigan, Aeronautical Research Center, Willow Run Airport, Ypsilanti, Michigan	
	Mr. R. F. May	
1	University of Texas	Development Contract Officer
	Defense Research Laboratory	VIA 500 East 24th Street
	Austin, Texas	Austin, Texas
2	Consolidated Vultee Aircraft Corp.	Development Contract Officer
	Ordnance Aerophysics Laboratory	VIA Consolidated Vultee Aircraft
	Daingerfield, Texas	Corporation
	Mr. J. E. Arnold	Daingerfield, Texas
1	General Electric Company	Army Ordnance Liaison
	Project HERMES	VIA Officer
	Schenectady, New York	Building 23
1	Mr. C. K. Bauer	General Electric Company
		Schenectady, New York
1	Douglas Aircraft Co., 3000 Ocean Boulevard, Santa Monica, Calif.	
1	Mr. E. F. Burton	
1	The Franklin Institute Laboratories	Inspector of Navy Material
	for Research and Development	VIA Room 1003
	Philadelphia, Pennsylvania	New Custom House Building
1	Mr. R. H. McClarren	Philadelphia 6, Penna.

BASIC AERODYNAMICS (X2) (Cont.)

- | | | |
|---|---|--|
| 1 | Eastman Kodak Company
Navy Ordnance Division
Rochester, New York | Naval Inspector of Ordnance
VIA Navy Ordnance Division
Eastman Kodak Company
50 West Main Street
Rochester 14, N. Y. |
| 1 | Director
California Institute of Technology
Jet Propulsion Laboratory
Pasadena, California | District Chief
Los Angeles Ordnance District
VIA 35 North Raymond Avenue
Pasadena, 1, California |
| 2 | Naval Attache for Research, American Embassy, Navy 100, c/o
Fleet Post Office, New York, N. Y. | |
| 1 | University of Calif. Dept. of Engineering, Berkeley, Calif.,
Prof. R. G. Folsom | |
| 1 | Cornell University, Dept. of Aeronautical Engineering, Ithaca,
New York, Prof. W. Sears | |
| 1 | Hughes Aircraft Co., Florence Avenue at Teal St., Culver City,
Calif., Attn: Mr. R. E. Hopper | |
| 1 | Dr. A. E. Puckett | |
| 1 | Director, Evans Signal Laboratory, Belmont, New Jersey
Attn: Chief, Service Branch | |
| 2 | Director, Guggenheim Aeronautical Lab., Calif. Institute of
Technology, Pasadena, California | |
| 1 | Princeton U., Dept. of Aeronautical Engineering, Princeton, N. J.
Prof. L. Lees | |
| 1 | Director, University of Maryland, Institute for Fluid Dynamics
and Applied Mathematics | |

*NOL CONSULTANTS

- | | |
|---|--|
| 1 | University of Virginia, Dept. of Physics, Charlottesville, Va.,
Prof. J. W. Beams |
| 1 | Harvard University, 21 Vanserg Bldg. Cambridge 38, Mass.,
Prof. G. Birkhoff |
| 1 | Dr. W. Bollay, Box 89, Downey, California |
| 1 | Johns Hopkins University, Dept. of Aeronautics, Baltimore 18,
Maryland, Dr. F. H. Clauser |
| 1 | New York U., Institute for Math. and Mechanics, 45 Fourth
Avenue, New York 3, N. Y., Prof. R. Courant |

BASIC AERODYNAMICS (X2)(Cont.)

- 1 Harvard University, Pierce Hall, Cambridge 38, Mass.,
Prof. H. W. Emmons
- 1 University of Wisconsin, Dept. of Chemistry, Madison, Wisconsin,
Prof. J. O. Hirschfelder
- 1 Princeton University, Palmer Physical Lab., Princeton, N. J.,
Prof. R. Ladenburg
- 1 Calif. Institute of Technology, Guggenheim Aeronautical Lab.,
Pasadena, Calif., Prof. H. W. Liepmann
- 1 The Institute for Advanced Study, Princeton, N. J.
Prof. J. von Neumann
- 1 University of Michigan, Dept. of Aeronautical Engineering,
Ann Arbor, Michigan, Prof. A. Kuethe
- 1 Dr. Gordon N. Patterson, 17 Langmuir Crescent, Langmuir
Crescent, Toronto 9, Ontario, Canada
- 1 Arnold Research Organization, Inc., Room 210, 522 Olive St.,
St. Louis, Missouri, Mr. Ronald Smelt
- 1 Harvard University, 109 Pierce Hall, Cambridge 38, Mass.,
Prof. R. von Mises,
- *1 Superintendent, U. S. Naval Postgraduate School, Naval
Academy, Annapolis, Md.
- 1 Central Air Documents Office, Wright-Patterson Air Force Base,
Dayton, Ohio
- 1 Chief of Naval Research, c/o Library of Congress, Technical
Information Section, Washington 25, D. C.
- 1 Commanding General, Air Material Command, Wright Field, Dayton, Ohio
F. Wattendorf
- 1 Cornell University, Dept. of Aeronautical Engineering, Ithaca, N.Y.
A. Kantrowitz
- 1 Calif. Institute of Technology, Guggenheim Aeronautical Lab.,
Pasadena, Calif., H. Nagamatsu

